Estimation of Gas-Production Potential Using Well Logs, Cretaceous of Northern Montana

Scientific Investigations Report 2005-5082

U.S. Department of the Interior
U.S. Geological Survey

Estimation of Gas-Production Potential Using Well Logs, Cretaceous of Northern Montana

By Timothy C. Hester

Scientific Investigations Report 2005-5082

U.S. Department of the Interior
U.S. Geological Survey

U.S. Department of the Interior
Gale A. Norton, Secretary

U.S. Geological Survey
P. Patrick Leahy, Acting Director

U.S. Geological Survey, Reston, Virginia: 2006

Posted online January 2006
Version 1.0

This publication is only available online at
http://pubs.usgs.gov/sir/2005/5082/

For more information about the USGS and its products:
Telephone: 1-888-ASK-USGS
World Wide Web: http://www.usgs.gov/

Any use of trade, product, or firm names in this publication is for descriptive purposes only and does not imply endorsement by the U.S. Government.

Although this report is in the public domain, it contains copyrighted materials that are noted in the text. Permission to reproduce those items must be secured from the individual copyright owners.

Suggested citation:
Hester, T.C., 2006, Estimation of gas-production potential using well logs, Cretaceous of northern Montana: U.S. Geological Survey Scientific Investigations Report 2005-5082, 27 p.

Contents

Abstract 1
Introduction 1
The Gas Effect 2
The N – D versus GR Crossplot 3
This Report 4
Geologic Setting 4
Data Set 5
Gamma-Ray, Neutron, and Density Tool Response 5
Effect of Clay 5
Effect of Gas 11
Calibration of the Gas Effect 11
Index System 12
The Effect of Clay on Porosity and Gas Production 13
Algorithms for Generating GPI Values 16
Using the Algorithm in Prizm 17
Lines on the Left Side of the Crossplot 20
Lines on the Right Side of the Crossplot 21
Using the Algorithm in Excel 22
Summary 23
Selected References 24
Appendix 1. Plug-in Algorithm for Calculating GPI Using Prizm 26
Appendix 2. Four Steps to Calculating Gas-Production Index Using Excel 27

Figures

1. Index map of Montana 2
2. Crossplot of neutron porosity minus density porosity versus gamma-ray intensity, showing hypothetical data from logged intervals and hypothetical liquid line 3
3. Neutron porosity minus density porosity versus gamma-ray intensity crossplot, showing values of gas-production index 3
4. Generalized stratigraphic column, showing Cretaceous units in northern Montana 4
5. Generalized block diagram (dual-water model) 4
6. Neutron porosity versus gamma-ray intensity 7
7. Neutron porosity minus density porosity versus gamma-ray intensity 8
8. Neutron porosity minus density porosity versus gamma-ray intensity and gas-production index 9
9. Density porosity versus gamma-ray intensity 10
10. Gas production (peak calendar year) versus gamma-ray intensity for 28 wells in northern Montana 14

11. Gas production (peak calendar year) versus gas-production index (GPI) for 28 wells in northern Montana 15
12–14. Prizm results:
12. Well no. 2....16
13. Well no. 6....17
14. Well no. 34....18
15. Neutron porosity minus density porosity versus gamma-ray intensity crossplot, showing equations for line segments that make up the gas-production index....19
16. Example of Excel spreadsheet 22
17. Summary crossplot of neutron porosity minus density porosity versus gamma-ray intensity 23

Table

1. Identification of 53 gas-producing wells in north-central Montana from which well-log and production data were obtained....6

Conversion Factors

Multiply	By	To obtain
inch (in.)	2.54	centimeter (cm)
inch (in.)	25.4	millimeter (mm)

Estimation of Gas-Production Potential Using Well Logs, Cretaceous of Northern Montana

By Timothy C. Hester

Abstract

Cretaceous sandstones of east-central Alberta and southern Saskatchewan, Canada, and eastern Montana, western North Dakota, and parts of South Dakota and Wyoming, United States, are recognized as a major source of natural gas. Estimates of recoverable biogenic methane from these rocks in the United States are as high as several trillions of cubic feet. In northern Montana, current gas production is localized around a few major structural features and is not well established in other areas. Although the potential for production exists, the lack of commercial development is due to three major factors: (1) the lack of pipeline infrastructure, (2) the lack of predictable and reliable rates of production, and (3) the difficulty in recognizing and selecting potentially productive gas-charged intervals.

Unconventional (tight), continuous-type reservoirs, such as those in the Cretaceous of the northern Great Plains, are not well suited for formation evaluation by conventional methods. Pay zones frequently consist only of thinly laminated intervals of sandstone, siltstone, shale, and disseminated clay. Potential producing intervals are commonly unrecognizable on standard suites of well logs and thus can be overlooked. To aid in the identification and selection of potential gas-producing intervals, an index is developed here that empirically links the "gas effect" (a geophysical-tool response to gas in a formation) to gas production. The index combines the effects of porosity, water saturation, and clay into a single value—the "gas-production index" (GPI)—that relates in situ rock and fluids to gas-production potential. The fundamental method for isolating the gas effect for calibration is to use a crossplot of neutron porosity minus density porosity (N – D) versus gamma-ray intensity (GR). In addition, an algorithm is developed to allow generation of the GPI by computer using digital well logs.

Well-log and gas-production data used for this study consist of 242 gas-producing intervals from 53 gas-producing wells located within a five-county area in north-central Montana. Interval depths range from ≈250 to 2,400 ft. Gas volumes in the peak calendar year of production range from ≈4 to 136 million cubic feet (MMCF). Nine producing rock units are represented in the data set. Producing-interval data show that porosity and gas production are closely linked to clay volume (the amount of clay measured at a given logged interval, as defined by Heslop). Highest porosities and maximum gas production occur together at an intermediate clay content of ≈12 percent, which, in these rocks, corresponds to ≈60 American Petroleum Institute (API) units. As clay volume approaches or exceeds 35 percent (130 API units), minimum porosity required for production increases rapidly, and the number of potential producing intervals declines. Gas production from intervals where clay volume exceeds 50 percent is rare. However, regardless of clay content, effective porosities of less than ≈8 percent are probably inadequate for commercial gas production in these rocks.

Introduction

Cretaceous sandstones of the northern Great Plains contain a major natural gas resource in the United States and Canada (Rice and Shurr, 1980). The volume of technically recoverable, undiscovered biogenic methane (Rice, 1975; Rice and Claypool, 1981) is estimated to be several trillions of cubic feet (Dyman and others, 1995) in the United States part alone. In northern Montana, the area of this study (fig. 1), current gas production is localized around a few major structural features, whereas large areas between these structures remain virtually untested. The lack of development can be attributed to several major causes—the lack of gas pipeline and gathering systems (Rice and Spencer, 1995); the geologic nature of continuous-type gas accumulations, such as the low matrix permeability, the low recovery factor, and the highly unpredictable recovery rates (Schmoker, 1995); and the focus of this report, the inability to recognize gas-charged reservoirs (Rice and Spencer, 1995).

Unconventional (tight), clay-rich reservoirs, such as those in the Cretaceous of the northern Great Plains, are not well suited to conventional methods of formation evaluation. Potential pay zones are often poorly defined on geophysical well logs and thus overlooked. An easy-to-use system developed here links the "gas effect" (as seen on geophysical logs) with actual gas production, thereby simplifying the identification and selection of potential gas-producing intervals.

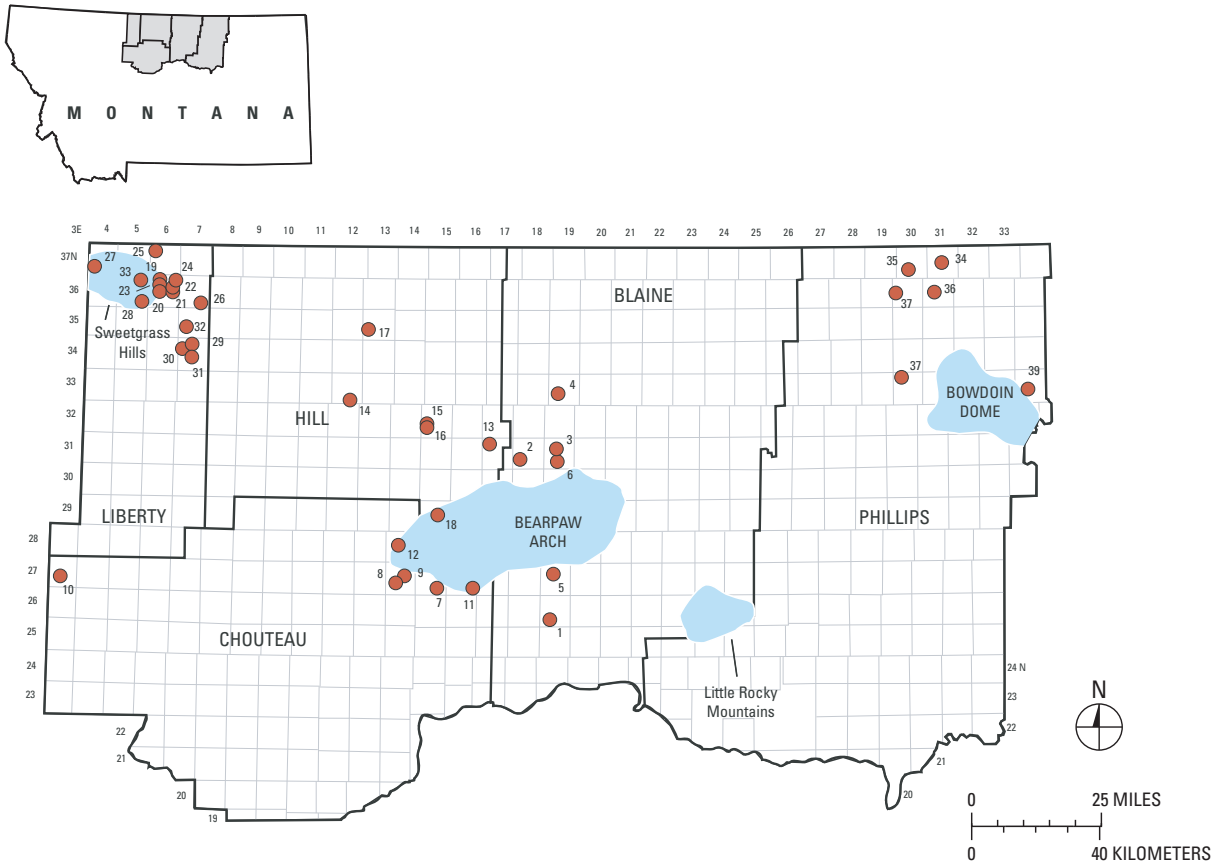

Figure 1. Index map of Montana, showing five-county study area, well locations, and major structural features. Wells are identified in table 1.

Geologic factors targeted by conventional log analyses—such as effective porosity, clay content, and water saturation—are combined and accounted for empirically by using a single "gas-production index" (GPI). The GPI, introduced here for the first time, in effect links log-derived, in situ rock properties with gas-production potential. The fundamental method for isolating the gas effect for calibration is the use of a crossplot of neutron porosity minus density porosity (N – D) versus gamma-ray intensity (GR), which was introduced in the early 1970s with the commercial availability of the compensated neutron and density wireline logging tools. An algorithm, discussed later in this report, allows computer generation of the GPI when digital well data are available.

The Gas Effect

The "gas effect" is a geophysical-tool response to gas in a rock unit. On well logs, the gas effect is most often manifested as a visual "crossover" of neutron-porosity and density-porosity curves. This crossover serves an important role in gas exploration. However, as clay content and associated bound water increase, the neutron-porosity and density-porosity curves separate until the crossover no longer occurs. The gas effect, though still present, is no longer detectable on these well logs. An effective method for detecting the gas effect in this situation is the use of a crossplot of N – D versus GR (fig. 2). The crossplot serves to separate porosity due to the gas effect from that due to clay and associated bound water. In this way, the gas effect—i.e., the presence of gas as shown by the crossover of well-log curves on the crossplot—is revealed without regard to clay content (Hester, 1999a). The approach to interpreting such a crossplot is explained further in the next section.

The magnitude of the gas effect is closely related to the bulk volume of gas present in the rocks surrounding the borehole. Thus, the gas effect is an indirect measure of gas-charged porosity and may substitute for water-saturation determinations as a qualitative measure of gas concentration and as an indicator of production potential. An index system, which is part of the crossplot (fig. 3), measures and scales the gas effect into 12 levels of magnitude (Hester, 1999a). The values of the index, referred to here as the "gas-production index" (GPI), are linked to actual gas production. In this way, the GPI provides an estimate of gas-production potential for a broad range of reservoir conditions.

The gas-production index is a robust indicator of gas-production potential. The index has been specifically calibrated for shallow gas-bearing sandstone reservoirs of the northern Great Plains (Hester, 1999a). Figure 4 shows the stratigraphic positions of the gas-producing units represented in the data of this report.

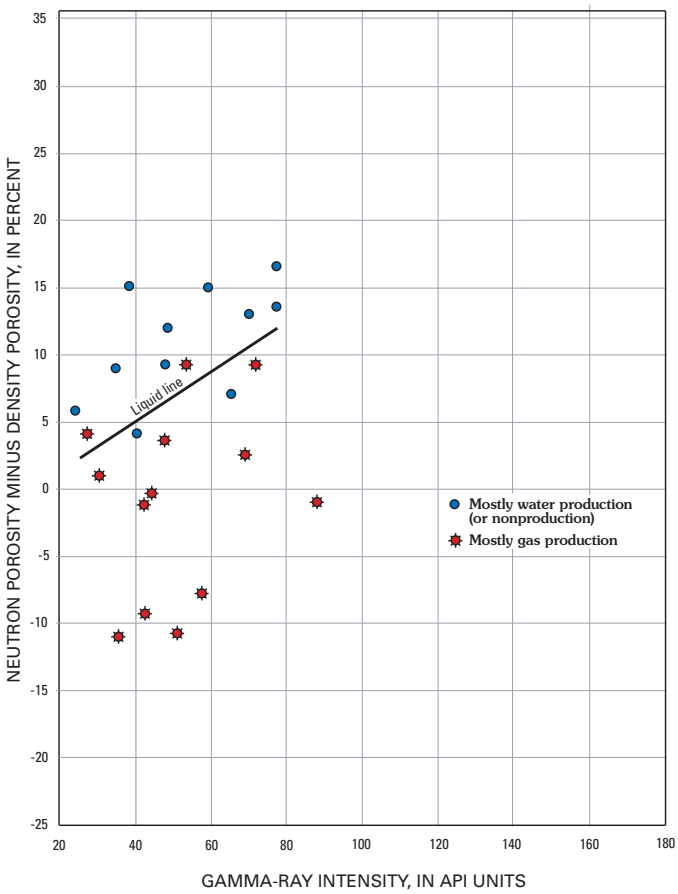

Figure 2. Crossplot of neutron porosity minus density porosity versus gamma-ray intensity, showing hypothetical data from logged intervals and hypothetical liquid line, which separates gas- from water-producing (or nonproducing) stratigraphic intervals.

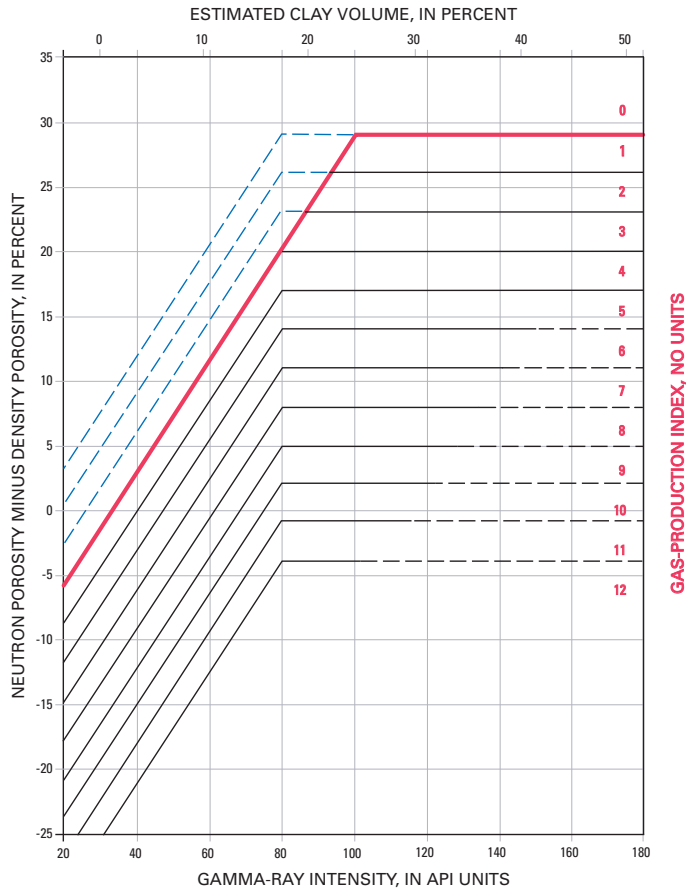

Figure 3. Neutron porosity minus density porosity versus gamma-ray intensity crossplot (N – D versus GR), with intervals between thin, solid lines showing values of gas-production index ranging from 0 to 12. Index is composed of empirical (hand drawn) zero-production baseline (heavy, red diagonal and horizontal line segments) with 12 levels of gas-production potential (thin diagonal and horizontal lines, dashed where inferred). The heavy red line represents an economic limit. Stratigraphic intervals whose data plot above this line are unlikely to deliver commercial volumes of gas. Level 1 indicates the least potential for gas production; level 12 indicates the greatest potential. Estimated clay volume is scaled opposite gamma-ray intensity (*x*-axis).

The N – D versus GR Crossplot

The relationship of neutron, density, and gamma-ray tool responses to the presence of clay and gas in a rock unit is expressed graphically (fig. 2) by plotting the difference between neutron and density porosity (N – D, *y*-axis) against gamma-ray intensity (GR, *x*-axis). This method has been used in the past to distinguish gas- from water-producing intervals in very shaly formations where conventional log analyses are ineffective. The inventor of this crossplot and specifically how it came into popular use are not documented in the literature. Case histories document the utility of the crossplot as a gas-detection tool in the Viking Formation of east-central Alberta, Canada (Cutress, 1974), and in numerous Cretaceous gas-bearing sandstones of northern Montana (Campen, 1975).

Successful application of the crossplot (as used previously) depends on the existence, close proximity, and identification of water-saturated zones with geologic and production characteristics similar to those of prospective gas-producing intervals. Log measurements from the water-saturated zones are plotted to establish a “liquid line” (Cutress, 1974; Campen, 1975), which then serves to separate gas- from water-producing (or nonproducing) intervals. Gas-bearing zones with production potential plot below the liquid line. The departure of the gas-bearing zones from the liquid line is the “gas effect,” a term that refers to the well-known opposing response of neutron- and density-porosity curves to the presence of gas in the formation. Typically, a liquid line is constructed for each formation of interest in a local area. The ideal position of the liquid line is commonly difficult to establish and may vary depending upon porosity, the degree of water saturation, and economic or production criteria specific to the formation or operator. Figure 2 shows a schematic N – D versus GR crossplot with a hypothetical liquid line and hypothetical producing-interval data.

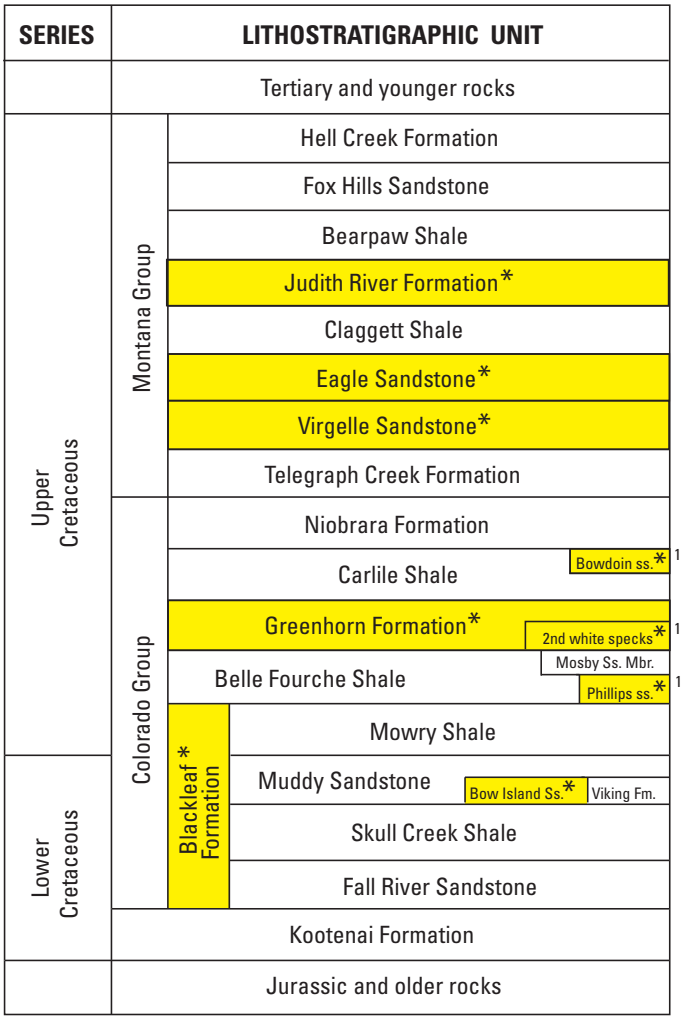

Figure 4. Generalized stratigraphic column, showing Cretaceous units in northern Montana (based on Rice, 1981). The yellow units with asterisks are gas-producing units in this region. The yellow units with superscript ones are named according to subsurface usage.

In the unconventional, continuous-type (Schmoker, 1995) gas accumulations of the northern Great Plains, 100 percent water-saturated zones are relatively uncommon. In addition, existing water-bearing sandstones are not always adjacent to prospective production, similar in clay content, or easily recognizable on well logs. Regional studies over broad geographic areas or investigations involving multiple formations are additionally complicated by the difficulties in constructing and interpreting multiple liquid lines.

A simple, more robust system of gas detection in shaly sandstones is developed here. The new system uses the same N – D versus GR crossplot, but eliminates the need to construct liquid lines for each formation and thus permits the investigator to compare formations with varying geologic characteristics at the same time. In addition, the systematic functioning of the crossplot (detailed in a following section) allows the plotted distribution of gas-bearing intervals to be explained in terms of relative variation in porosity and water saturation, clay content, bound water, and production potential. Thus, the crossplot becomes an interpretive tool in support of (or in lieu of) conventional formation evaluation.

This Report

This report is a compilation of several published reports and abstracts (Hester, 1999a, 1999b, 1999c, 1999d, 2001). An overview of northern Great Plains geology and a description of the data set are followed by a brief review of the geophysical-tool response to clay and gas. The two variables N – D and GR in the crossplot are discussed in terms of rock constituents, fluids, and effective and total porosity by using the dual-water model (fig. 5), modified from that shown schematically by Schlumberger (1987). Calibration of the gas effect is then explained and integrated with some geologic interpretations. Finally, the algorithm used to generate the GPI is described for two different computer applications—Geographix's Prizm, a log-analysis program specifically designed for digital well-log files, and Microsoft's Excel spreadsheet software. Each computer application requires a slightly different version of the algorithm and therefore is discussed separately. The descriptions include enough detail to give the user the flexibility to modify the algorithm, if necessary, for use in other similar software programs. Appendixes 1 and 2 explain how to enter the algorithm directly into either Prizm or Excel, respectively.

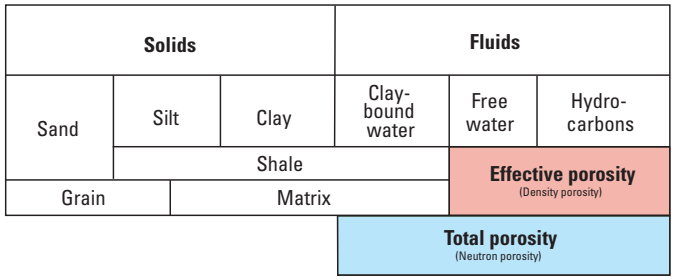

Figure 5. Generalized block diagram (dual-water model) showing schematic relationship of solid and fluid constituents of shaly formations. (Modified from Schlumberger, 1987.)

Geologic Setting

Cretaceous rocks of the Western Interior were deposited along a north-trending inland sea that extended from the Gulf of Mexico to the Arctic Ocean (Rice and Shurr, 1980). Cretaceous strata are widespread along the trend. Large parts of the stratigraphic section are preserved in isolated structural basins well known for coal, oil, and gas resources (Molenaar and Rice, 1988). The Cretaceous strata of northern Montana (the focus of this report, fig. 4) were deposited along the western shelf edge of this trend and are characterized by the low-permeability

(tight) marine and continental sandstones and shales that are more or less typical of the Cretaceous in general. Occupying most of the stratigraphic section and underlying much of east-central Alberta and southern Saskatchewan, eastern Montana, western North Dakota, and parts of South Dakota and Wyoming is a potentially vast, low-pressure, continuous-type (unconventional) natural gas reservoir (Schmoker, 1995; Shurr and Ridgley, 2002). In this area, within only a few thousand feet of the surface, the potential exists for recovering large volumes of gas.

In the northern Great Plains, structural relief is generally low. Where obvious structure exists, gas production is concentrated. Producing formations are primarily marine-shelf sandstones (Rice, 1981) that range from relatively clean to highly silt and clay rich. Pay zones commonly consist of thinly laminated intervals primarily classified as sandstone, siltstone, and shale, although any lamina of the sandstone or siltstone or shale—or a combination of the three in total—may contain large amounts (approaching 50 percent) of disseminated clay (Henry, 1979; Kukal, 1981). Low-permeability, high-clay-content zones such as these may be commercially producible, but they are commonly not recognized as such on geophysical well logs and are not well suited to conventional methods of formation evaluation. Clay-rich, low-permeability strata tend to suppress resistivity (Whitney and Ahlbrandt, 1996) and spontaneous-potential curve deflections (Schlumberger, 1987), making saturation determinations unreliable (Kowalchuk and others, 1974). In the calibration described here, the effects of clay and water saturation are empirically accounted for, and production potential is linked directly to the gas effect.

Data Set

The data for this report consist of log-derived geophysical and gas-production data from 53 wells (fig. 1; table 1) located within a five-county area of north-central Montana. Wells were selected to provide the necessary log suite and to represent the producing formations and broad range of geologic conditions that exist within the study area. Each well has some measure of demonstrated production. However, of the 53 wells, only 28 were active as of 1999 or have produced significant amounts of gas for at least two calendar years. Eleven wells recorded some measure of initial production but were then either shut in or abandoned. Fourteen other wells (unidentified by well name, location, or other identifying labels, except for production zone and interval number) are represented only by tabulated geophysical data (Campen, 1975). In total, nine Cretaceous gas-producing units (fig. 4) are represented.

Geophysical data for each of 242 gas-producing intervals (in the 53 wells) include neutron and density porosity, gamma-ray intensity, depth, and interval thickness. Only gas-producing intervals were selected for analysis, and all perforated intervals in the producing zone of each of the 53 wells were included. The number and thickness of intervals were determined on the basis of uniform log character. Log curves were averaged through each interval where practical; otherwise, the most optimistic value was recorded. Compensated neutron and density logs were run on a sandstone matrix in which matrix density (ρ_{ma}) equals 2.65 g/cm^3 and fluid density (ρ_f) equals 1.0 g/cm^3. Interval depths range from ≈250 to 2,400 ft.

Gas-production data used in the calibration of the gas effect are from commercially available, digital, well-production databases. Producing wells commonly incorporate multiple perforated intervals (table 1). A particular interval may or may not contribute to production. Therefore, quantitative gas-production data are associated only with well production, not with individual intervals. The interval data (53 wells, 242 intervals) are used to define an empirical boundary that distinguishes gas from water production (or nonproduction) and also establishes a baseline from which to measure the gas effect. The 28 wells described above (those with at least two consecutive years of cumulative production history; 159 intervals) are used to link the gas effect to longer-term (well) production and to establish a range of production volumes typical for a given level of gas effect under more or less normal conditions. For each of these 28 wells, interval data are averaged, weighted by thickness, and paired with the volume of gas produced in the peak calendar year of production for that well.

Gamma-Ray, Neutron, and Density Tool Response

The relationships among gamma-ray, neutron, and density tool responses are used (1) to empirically account for clay, porosity, and water saturation and (2) to isolate the gas effect in a useful and predictable way. Understanding the relationships is an important part of linking the neutron minus density (N – D) versus gamma-ray intensity (GR) crossplot with geology, calibrating the gas effect, and developing the crossplot as an analysis tool for making basic interpretations of the data. To that end, tool response to clay and gas and the crossplot variables N – D and GR are explained and linked with the dual-water model (fig. 5). In this model the term “effective porosity” includes porosity filled by free (movable) water and hydrocarbons. “Total porosity” includes effective porosity and clay-bound (immovable) water (fig. 5).

Effect of Clay

Heslop (1974) showed that in shaly sandstones, GR increases linearly with clay volume. Clay volume is measured independently of “shale” volume by using relative GR deflections (that is, percentages) converted to API units. Clay volume is important because of its effect on porosity, permeability, and geophysical-tool response. Because Heslop’s GR data were limited to an upper value of ≈100 API units, he was unable to establish an upper limit for his linear trend; he therefore suggested that his clay-volume estimates were probably high (Heslop, 1974).

Table 1. Identification of 53 gas-producing wells in north-central Montana from which well-log and production data were obtained.

[Well numbers refer to locations shown in figure 1. Well information and producing units are as shown on well-log headers and completion cards. Well data from PI/Dwights PLUS Well Data (on CD-ROM [1999 update]) available from IHS Energy Group]

Well no.	Operator	Lease name and no.	Location	Producing unit	No. of intervals	
			Blaine County			
1	Tricentrol USA	O'Connell 29-4	sec. 29, T. 26 N., R. 19 E.	Judith River	4	
2	Tricentrol USA	Ramberg 19-5	sec. 19, T. 31 N., R. 18 E.	Judith River	3	*
3	Montana Power	Sprinkle 9-9	sec. 09, T. 31 N., R. 19 E.	Judith River	5	*
4	Probe Oil	Putnam 1	sec. 20, T. 33 N., R. 19 E.	Judith River	1	
5	Roland Bond	Elizabeth Campbell 2-9	sec. 09, T. 27 N., R. 19 E.	Eagle	1	
6	High Crest Oil	Roberts 28-4	sec. 28, T. 31 N., R. 19 E.	Eagle	3	*
			Chouteau County			
7	Montana Power	IX Ranch B9-26	sec. 26, T. 27 N., R. 15 E.	Judith River	2	*
8	Montana Power	State 5-20	sec. 20, T. 27 N., R. 14 E.	Virgelle	7	*
9	Viking Resources	State 2-15	sec. 15, T. 27 N., R. 14 E.	Virgelle	2	*
10	Monterrey Petroleum	Sada Woods 1-21	sec. 21, T. 27 N., R. 03 E.	Bow Island	4	*
11	Montana Power	Weaver 4-25	sec. 25, T. 27 N., R. 16 E.	Eagle	13	*
12	Montana Power	State 6	sec. 16, T. 28 N., R. 14 E.	Eagle	11	*
			Hill County			
13	Norfolk Energy	Clark 1-14	sec. 01, T. 31 N., R. 17 E.	Judith River	1	*
14	Concept Resources	Givan 3-34	sec. 34, T. 33 N., R. 12 E.	Judith River	6	
15	Montana Power	Runkel 16-19	sec. 19, T. 32 N., R. 15 E.	Virgelle	3	*
16	Montana Power	Runkel 13-19	sec. 19, T. 32 N., R. 15 E.	Virgelle	1	*
17	Oil Resources Inc	Larson 19-4	sec. 19, T. 35 N., R. 13 E.	2nd white specks	3	
18	Roland Bond	Rocky Boy 1-15	sec. 15, T. 29 N., R. 15 E.	Eagle	5	*
			Liberty County			
19	Montana Power	Bingham-Anderson 1-4	sec. 04, T. 36 N., R. 06 E.	2nd white specks	4	*
20	Montana Power	State 1-16	sec. 16, T. 36 N., R. 06 E.	Blackleaf	10	
21	Montana Power	Johns 7-15	sec. 15, T. 36 N., R. 06 E.	Blackleaf	4	*
22	Montana Power	Gunderson 7-10	sec. 10, T. 36 N., R. 06 E.	Blackleaf	2	*
23	Lawrence McCarthy	Gunderson 1-9	sec. 09, T. 36 N., R. 06 E.	Blackleaf	11	
24	Montana Power	E Gunderson 14-2	sec. 02, T. 36 N., R. 06 E.	Blackleaf	4	
25	Kenneth Luff	Federal 1-6	sec. 06, T. 37 N., R. 06 E.	Blackleaf	4	
26	Lawrence McCarthy	Hodges 1-34	sec. 34, T. 36 N., R. 07 E.	2nd white specks	21	*
27	Croft Petroleum	Brown 1	sec. 30, T. 37 N., R. 04 E.	Bow Island	2	*
28	JB Appling	Federal 7A-25	sec. 25, T. 36 N., R. 05 E.	Bow Island	3	*
29	Grace Petroleum	Milnar 4-7X	sec. 04, T. 34 N., R. 07 E.	Bow Island	3	*
30	Grace Petroleum	Graff 8-15	sec. 08, T. 34 N., R. 07 E.	Bow Island	5	*
31	Grace Petroleum	State 16-7	sec. 16, T. 34 N., R. 07 E.	Bow Island	1	*
32	Montana Power	Joy 9-20-35-7	sec. 20, T. 35 N., R. 07 E.	Bow Island	1	
33	Cardinal Petroleum	Jensen 11-1	sec. 01, T. 36 N., R. 05 E.	Blackleaf	4	*
			Phillips County			
34	Midlands Gas	State 1671-1	sec. 16, T. 37 N., R. 31 E.	Bowdoin	10	*
35	Midlands Gas	Fee 2970-1	sec. 29, T. 37 N., R. 30 E.	Bowdoin	9	*
36	Midlands Gas	Federal 1761-2	sec. 17, T. 36 N., R. 31 E.	Bowdoin	15	*
37	Midlands Gas	Federal 0530-1	sec. 05, T. 33 N., R. 30 E.	Phillips	3	
38	Southland Royalty	Federal 1860-1	sec. 18, T. 36 N., R. 30 E.	Bowdoin	14	*
39	Falcon-Colorado Exploration	Federal 2-21	sec. 21, T. 33 N., R. 34 E.	Phillips	2	*
			Tabulated interval data from Campen (1975)			
40–53					35	
				Total intervals	242	

* Intervals (159 total) in the wells with at least two-year production history (all other intervals had only initial production).

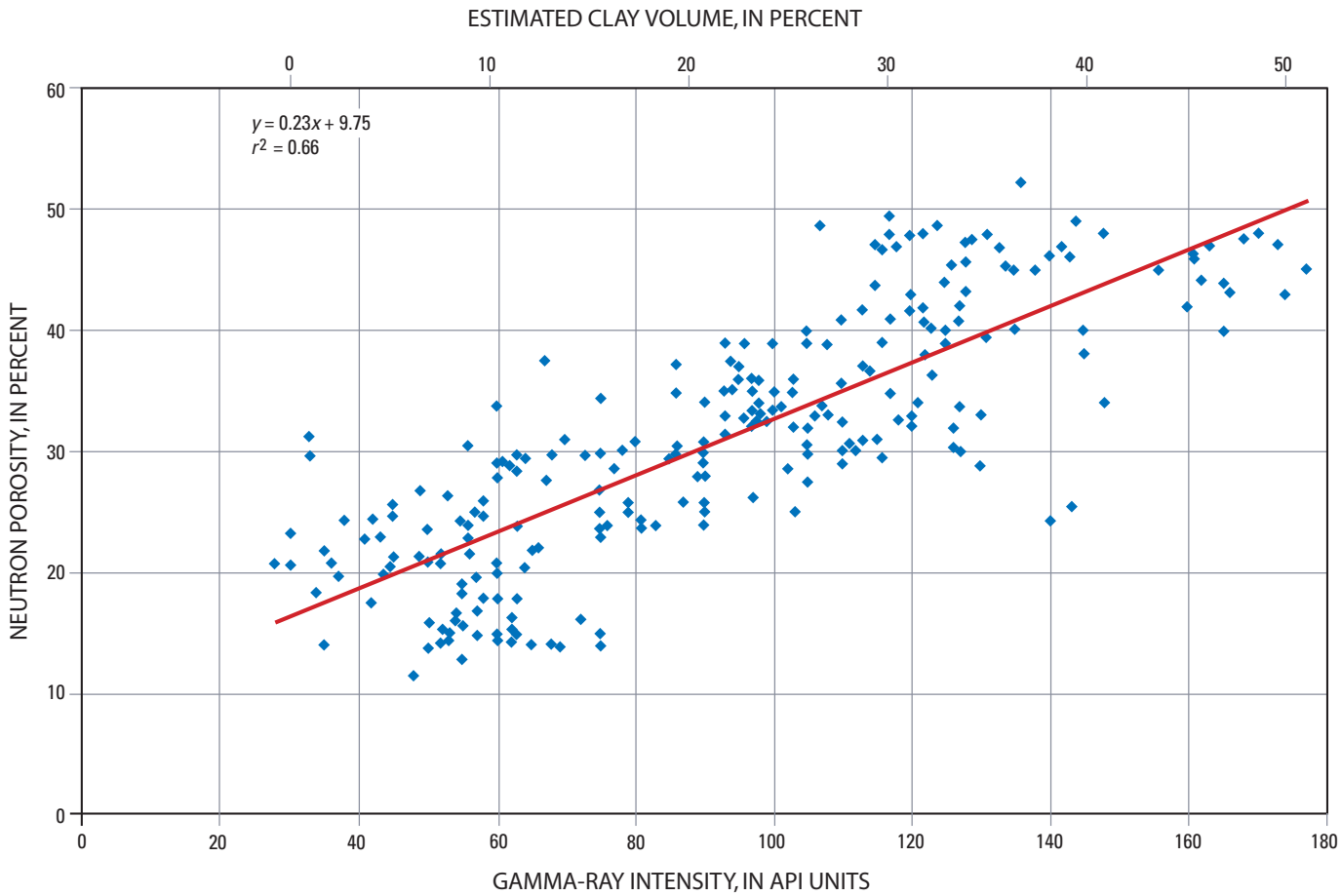

Figure 6. Neutron porosity versus gamma-ray intensity for all 242 perforated intervals studied in this report. Fifty-three wells are represented (table 1). Linear-regression line shows average neutron response to bound water associated with clay. Data scatter reflects variations in effective porosity and gas saturation. Estimated clay volume is scaled opposite gamma-ray intensity (*x*-axis). Equation and sample coefficient of determination (r^2) for regression line are shown in upper left corner.

The data set presented here includes GR values as high as 175 API units for intervals in the Bowdoin sandstone (an informal unit within the Carlile Shale), in which core and log data indicate a clay volume up to 50 percent (Henry, 1979; Kukal, 1981). By using these new data as an upper endpoint and applying Heslop's linear trend, a scale for estimated clay volume is shown opposite the GR axis in figures 6 through 9. This scale does not account for varying proportions of clay minerals with different intrinsic radioactivity levels.

Clay volume estimated in this way is a rough approximation, used here only for comparison and to investigate regional trends. As clay volume increases, bound water also increases. A linear relationship of bound water with clay volume is demonstrated in the next section. The following paragraphs outline the response of neutron- and density-porosity tools to the presence of clay and associated bound water.

The neutron tool responds primarily to hydrogen in the formation (Schlumberger, 1987). Hydrogen is a major component of saturating pore fluids (free water and hydrocarbons) and bound water associated with clay, but hydrogen may also be present in clay minerals in the form of hydroxyl ions (OH^-) or in nonporous hydrous minerals such as gypsum in the form of chemically attached water of crystallization (Schlumberger, 1987). Under normal circumstances, and in many producing formations consisting of clean sandstone, saturating pore fluids contribute overwhelmingly to the amount of hydrogen per unit volume (the hydrogen index). Thus, in most conventional, liquid-filled reservoirs, the neutron tool measures total porosity (fig. 5). The generalized neutron-porosity equation is

$$\phi_{NEUTRON} = \phi_{BW} + \phi_{FW} + \phi_{HC} = \phi_{TOTAL}\,, \qquad (1)$$

where

ϕ_{BW} = porosity filled with bound water (including water bound by surface tension),
ϕ_{FW} = porosity filled with free water, and
ϕ_{HC} = porosity filled with hydrocarbons.

Equation 1 reflects the response of the neutron tool to liquid-filled porosity in terms of the dual-water model (fig. 5).

The density tool responds primarily to electron density, which varies with formation bulk density (Schlumberger, 1987).

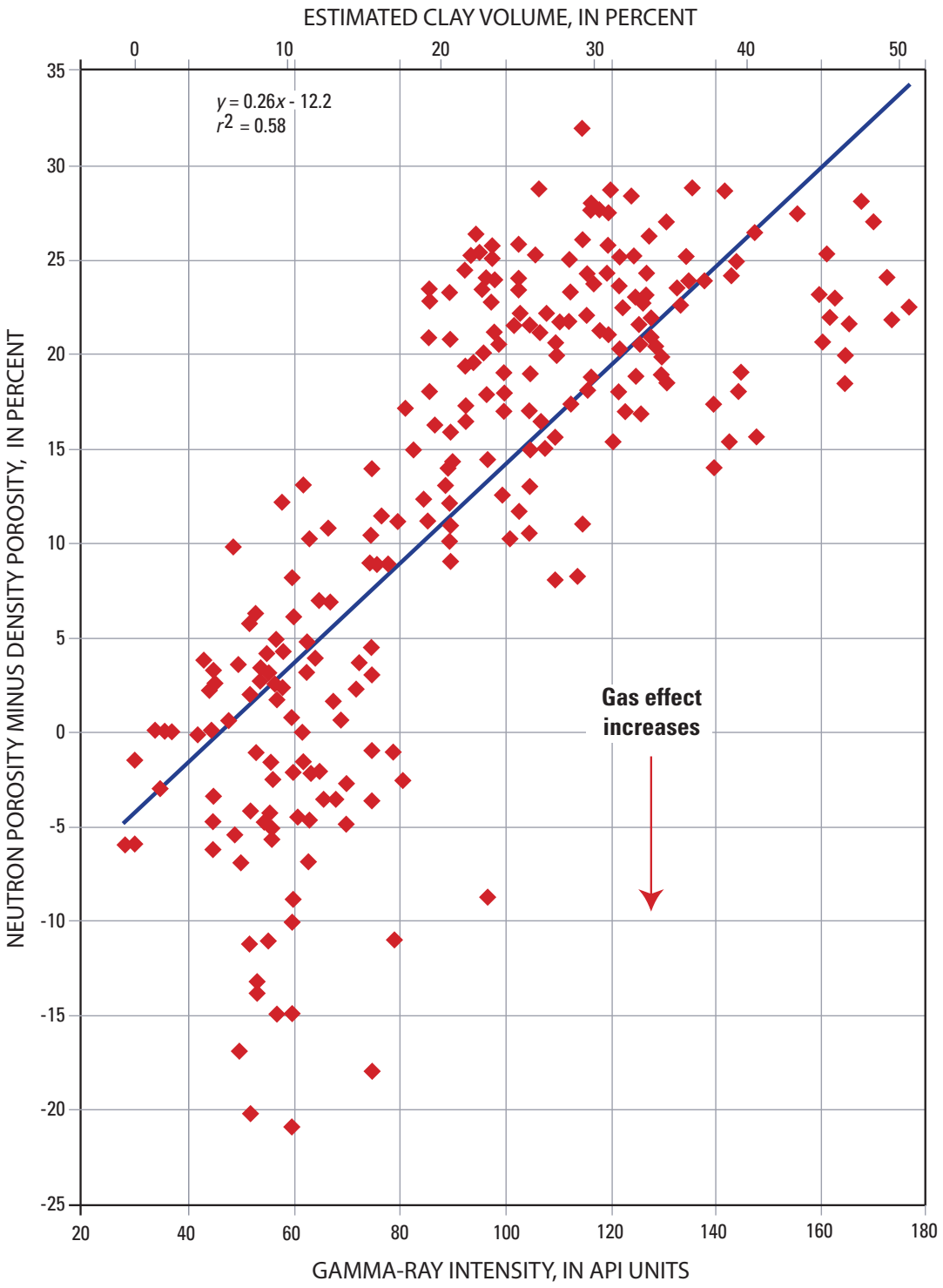

Figure 7. Neutron porosity minus density porosity versus gamma-ray intensity for all 242 gas-producing intervals of this report. Linear regression line shows average response of porosity associated with bound water (neutron porosity minus density porosity, N – D, *y*-axis [see fig. 5]) versus clay content (GR). Data scatter shows variations in the gas effect. Estimated clay volume is scaled opposite gamma-ray intensity (*x*-axis). Equation and sample coefficient of determination (r^2) for regression line are shown in upper left corner.

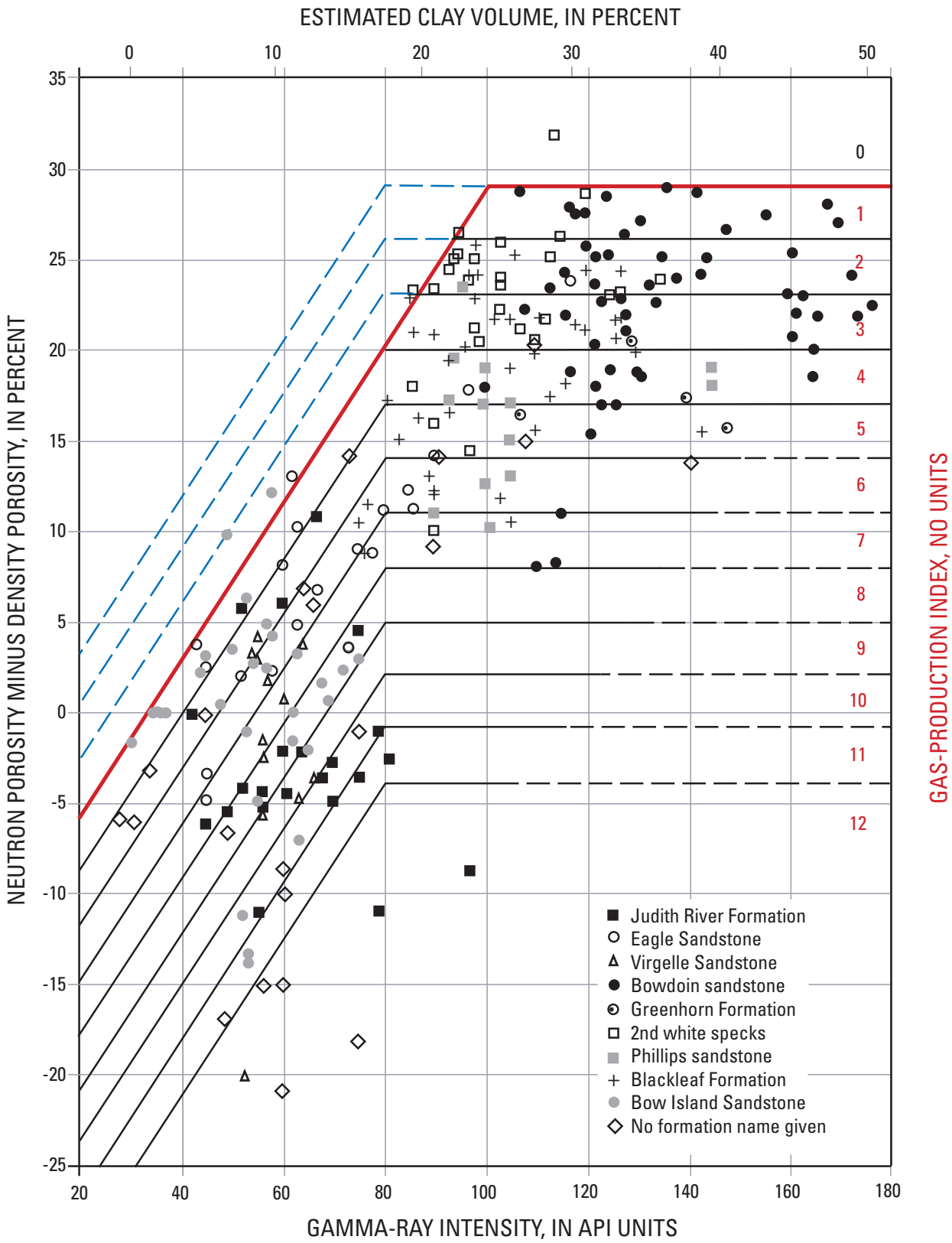

Figure 8. Neutron porosity minus density porosity versus gamma-ray intensity for all 242 gas-producing intervals studied in this report. Fifty-three wells are represented (table 1). Calibration system is composed of empirical (hand drawn) zero-production baseline (heavy, red diagonal and horizontal line segments) and 12 indexed levels of gas-production potential (bounded by thin diagonal and horizontal lines, dashed where inferred). Level 1 indicates the least potential for gas production; level 12 indicates the greatest potential. Estimated clay volume is scaled opposite gamma-ray intensity (*x*-axis).

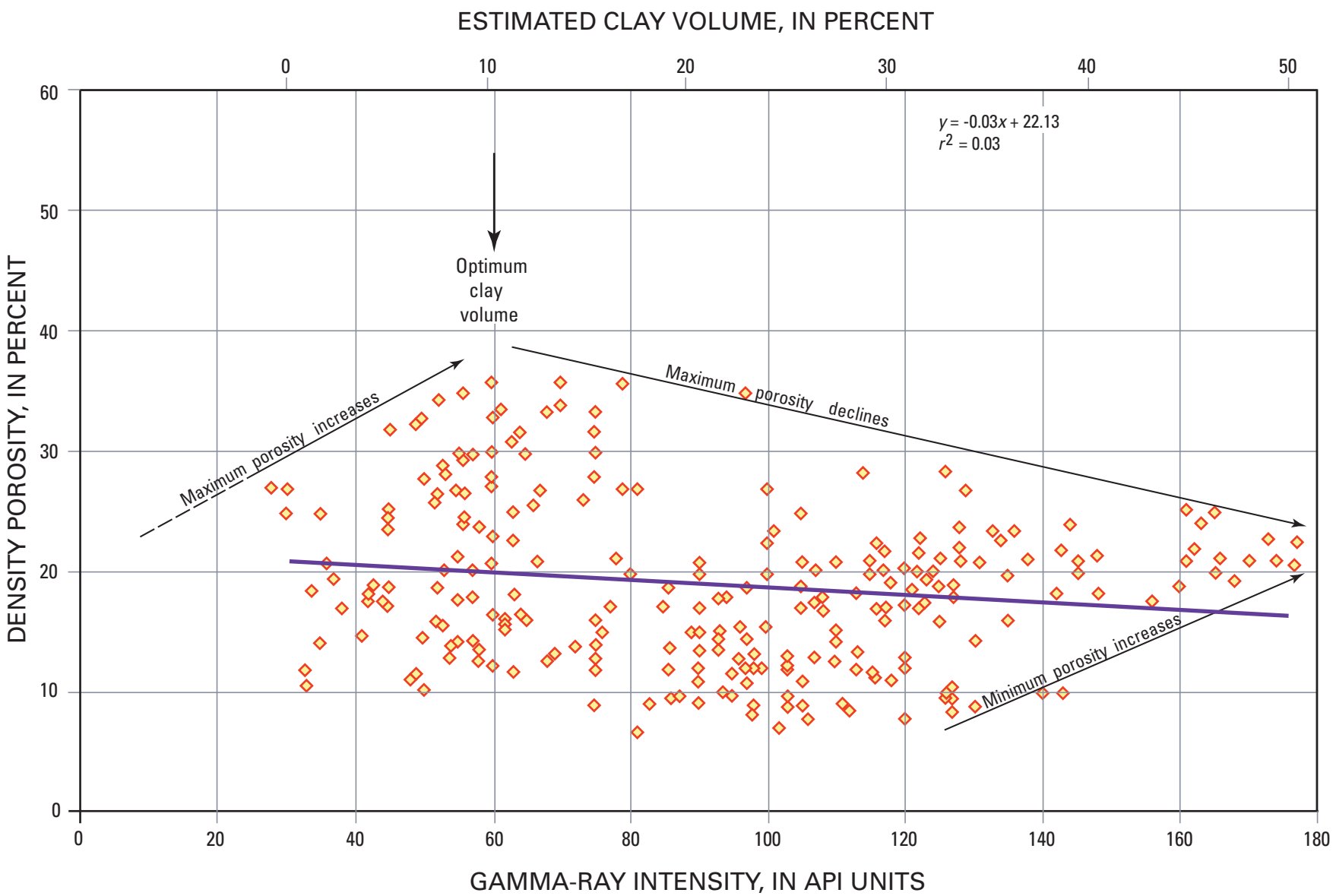

Figure 9. Density porosity versus gamma-ray intensity for all 242 gas-producing intervals studied in this report. Fifty-three wells are represented (table 1). Linear-regression line (heavy, blue solid line) shows average porosity of gas-producing intervals with increasing clay content. Estimated clay volume is scaled opposite gamma-ray intensity (*x*-axis). Equation and sample coefficient of determination (r^2) for regression line are shown in upper right corner.

Bulk-density measurements incorporate all formation constituents, including both solid and fluid components. Porosity is determined algebraically from such measurements by assigning values for matrix and fluid density. In formations for which lithology and fluid type are well known (and therefore matrix- and fluid-density values are correct), the density tool provides a reliable measure of effective porosity (fig. 5). The generalized density-porosity equation

$$\phi_{DENSITY} = \phi_{FW} + \phi_{HC} = \phi_{EFFECTIVE} \quad (2)$$

reflects the response of the density tool in terms of the dual-water model (fig. 5).

In formations with liquid-filled porosity (under ideal conditions and with correct matrix and fluid densities), the crossplot variable N – D (*y*-axis, fig. 2) empirically accounts for effective porosity (as shown by subtracting equations 1 and 2 and then combining terms):

$$\begin{aligned} N - D &= \phi_{NEUTRON} - \phi_{DENSITY} = \phi_N - \phi_D \\ &= (\phi_{BW} + \phi_{FW} + \phi_{HC}) - (\phi_{FW} + \phi_{HC}) = \phi_{BW} . \end{aligned} \quad (3)$$

Thus, the variable N – D reflects porosity associated with bound water.

Effect of Gas

The hydrogen index of liquid hydrocarbons is nearly that of water (Schlumberger, 1987). Therefore, the neutron tool measures total porosity in either oil- or water-filled formations. Gas, however, contains much less hydrogen per unit volume than water or liquid hydrocarbons and causes the neutron tool's measurements of the porosity values (ϕ_{HC}) to be too low. In addition, the excavation effect (Segesman and Liu, 1971) causes the neutron tool to measure a total porosity value that is even lower than that accounted for by the reduction in hydrogen index. The excavation effect is enhanced in combination with water (saturating or bound) and maximized at higher porosities and intermediate water saturations and (or) higher clay volumes. After correcting equation 1 for gas by subtracting the term $-(\phi_g + \phi_{EX})$,

$$\phi_N = \phi_{BW} + \phi_{FW} + \phi_{HC} - (\phi_g + \phi_{EX}) , \quad (4)$$

where

ϕ_g = porosity filled with gas and
ϕ_{EX} = the excavation effect.

The minus sign reflects a negative contribution, due to the presence of gas, to the porosity measurement by the neutron tool. Thus, neutron porosity in the presence of gas is a measure of total porosity minus the effect of gas and excavation.

When neutron porosity is plotted against clay content, the effects of bound water become apparent. The regression line of figure 6—a plot of neutron porosity versus GR (a measure of clay content) for all perforated intervals of the data set—shows a systematic, linear increase in neutron porosity as clay content increases. Neutron porosity increases as hydrogen associated with clay-bound water increases. In gas-charged formations, such as those represented by the data of figure 6, bound water is the primary contributor to the hydrogen index. Thus, the sample coefficient of determination ($r^2 = 0.66$) indicates that about two-thirds of the change in the neutron response is due to the linear increase of bound water associated with increasing clay content. Data scatter about the regression line reflects variations in effective porosity and gas saturation.

The densities of oil and water are similar compared to the density of natural gas, which is much lower. In the presence of gas (with all other variables being equal) the density tool measures a lower bulk density, which results in a corresponding higher porosity that is more or less proportional to the volume percent of gas present. If the term ϕ_G is added to equation 2,

$$\phi_D = \phi_{FW} + \phi_{HC} + \phi_G , \quad (5)$$

where

ϕ_G = the addition of apparent porosity to the density tool measurement as a result of gas in the formation.

Without adjustment to the fluid-density value to account for the lower density of the gas, the calculated effective porosity will be too high because it reflects the measurement of effective porosity plus gas-filled porosity.

In formations with gas-charged effective porosity, the variable N – D can be written (by subtracting equations 4 and 5 and combining terms) as

$$\begin{aligned} N - D = \phi_N - \phi_D &= (\phi_{BW} + \phi_{FW} + \phi_{HC} - \phi_g - \phi_{EX}) \\ &\quad - (\phi_{FW} + \phi_{HC} + \phi_G) \\ &= \phi_{BW} + \phi_{FW} + \phi_{HC} - \phi_g - \phi_{EX} - \phi_{FW} - \phi_{HC} - \phi_G \\ &= \phi_{BW} - \phi_g - \phi_{EX} - \phi_G \\ &= \phi_{BW} - (\phi_g + \phi_{EX} + \phi_G) . \end{aligned} \quad (6)$$

When the variable N – D is plotted against GR (fig. 2), bound water (ϕ_{BW}; equation 6) is empirically accounted for as a function of clay content, and vertical variation of the plotted data becomes a measure of the cumulative gas effect: $-(\phi_g + \phi_{EX} + \phi_G)$. The negative value reflects displacement below the liquid line (for example, fig. 2).

Calibration of the Gas Effect

The algebraic difference between neutron and density porosity (N – D) in liquid-filled formations is a measure of bound water (equation 3). In the presence of gas, N – D is a measure of bound water minus the gas effect (equation 6). When N – D is plotted against clay content (GR), the effects of bound water and gas are separated. Figure 7 shows all 159

gas-producing intervals of this report plotted on the N – D versus GR crossplot. The least-squares regression line shows the dependence of N – D on gamma-ray intensity. Clay content (Heslop, 1974) and bound water increase linearly with gamma-ray intensity. Thus, the sample coefficient of determination ($r^2 = 0.58$) indicates that more than half of the change in N – D is due to variation in clay content and associated bound water. Data scatter is due to variations in the magnitude of the gas effect.

The term "gas effect" refers to the opposing response of neutron- and density-porosity curves to the presence of gas in the formation. Some scatter, not related to in situ gas volume, is introduced by differing tool responses to porosity and by the irregular enhancement of excavation as porosity, water saturation, and clay content and clay-mineral type vary (Segesman and Liu, 1971). Therefore, the magnitude of the gas effect is closely, but not precisely, related to the absolute in situ volume of gas measured by the combination of the two porosity tools. The amount of variation is not easily quantified and thus imposes a limit on the degree of resolution possible for the gas effect. An intermediate index—the "GPI" (gas-production index)—is introduced here to compensate for that variation and to link the gas effect to production potential. Note the subtle but important conceptual difference between the gas effect and the GPI. The gas effect is a tool response to a given volume of in situ gas; the GPI is an indexed measure of the gas effect, calibrated with respect to actual production.

The basis for the system using the GPI consists of two fundamental components: (1) a baseline from which the gas effect can be measured (for example, a liquid line, fig. 2) and (2) an incremental (smoothing) system that maximizes resolution of the gas effect within the limits prescribed by the otherwise unaccounted-for variations in tool response and excavation. In this system, no water-bearing intervals or liquid lines as such are used. Instead, a "zero-production baseline" is empirically determined by using the 242 gas-producing intervals from the 53 wells of the production data set (table 1). This baseline represents an economic limit for commercial gas production and may vary through time as economic limits fluctuate in response to changing gas prices and technology. In this sense, the presence and position of the data on the crossplot empirically define the economic limits of gas production. The baseline so created is the cornerstone of the calibration system, which allows intervals or formations within a well, or from different wells, to be compared with each other in the context of production potential. Well data from anywhere in the region may be compared on the same crossplot.

Index System

The index system (figs. 3 and 8) consists of two sets of parallel lines positioned on the crossplot to conform to three fundamental ideas:

1. The absence of producing-interval data represents a theoretical "zero" economic production potential; therefore, the distribution of the data on the crossplot ultimately defines the limits of commercial gas production (in terms of the gas effect) for the region.
2. The gas effect increases vertically downward from these line segments in a systematic and predictable way.
3. There is a definable clay volume, above which gas production rapidly declines.

Two heavy, red line segments bound the data of figure 8 (all gas-producing intervals; table 1)—a diagonal line and a horizontal line. Both are hand drawn to include the maximum number of data points (≈98 percent) and minimize outliers. Straight-line segments are used (both diagonally and horizontally) because they better constrain the data throughout the range of GR values than do curved lines. The slopes and point of intersection (100 API units) of these heavy, red line segments are artifacts of an empirical "best fit" to the data. Together, these line segments establish a regional liquid line (without using water-bearing intervals) for all producing formations of northern Montana as a group and approximate the economic limit of commercial gas production. This empirical limit is referred to here as the "zero-production baseline." All other lines are parallel to these heavy, red line segments. Intervals that plot above this baseline are unlikely to deliver commercial volumes of gas.

Below the baseline, gas production without water is not guaranteed, but the potential for production increases with vertical displacement (decreasing N – D; increasing GPI; figs. 3, 7, and 8). The magnitude of displacement is measured by using a series of lines parallel to the zero-production baseline. These parallel lines envelop and subdivide the data and scale the gas effect into 12 levels of GPI. The levels are equally spaced in the vertical direction and numbered consecutively, increasing from top to bottom (note that the 12th level is open-ended). Level 1 has the least potential for gas production; level 12 has the greatest potential. Thus, GPI increases linearly as a function of the level occupied by a data point. This linear index reflects an assumed linear relationship of the gas effect to in situ gas volume. This assumption is not precisely the case, however, because the excavation effect varies in a nonlinear way as geologic conditions change. Thus, the cumulative gas effect may vary somewhat with factors other than the exact volume of gas present. The average excavation effect, for sandstone with 20 percent porosity (the trend for production-interval data of this report, fig. 9), may vary as much as three porosity units (Segesman and Liu, 1971). To account for this variation, allow for maximum resolution of the gas effect, and preserve the simplicity of the calibration system, each GPI level spans three porosity units, as measured along the N – D (y) axis.

The slope break for the parallel lines (80 API units) represents the point at which increasing clay content begins to rapidly degrade reservoir quality. This interpretation (discussed in the following section) is determined by the porosity and production data of this report and the porosity and clay-volume data of Schmoker (1997). Using the GPI levels, as opposed

to using porosity units of the *y*-axis (N – D), normalizes the gas effect with respect to the zero-production baseline. This approach allows intervals or stratigraphic units to be compared with each other without regard to clay content. In a given well, however, prospective producing intervals within the same zone of interest (for example, stratigraphic units) should be selected on the basis of low clay content. The cleanest intervals within any potential pay zone will best characterize the production potential for that zone.

The Effect of Clay on Porosity and Gas Production

Heslop (1974) showed that the gamma-ray intensity in shaly sandstones increases linearly with clay volume. Clay volume (as opposed to "shale" volume) is estimated by using relative gamma-ray deflections (that is, percentages) and converted to API units. Important in Heslop's correlation is a distinction between grain- and matrix-supported lithologies (sandstone and shale, respectively; fig. 5) and the position of the transition between them. In nature, the transition between these two endpoints is continuous. Here, the transition is represented by a fixed clay volume, marked on the N – D versus GR crossplot by the intersection of diagonal and horizontal lines (figs. 3 and 8; 80 API units). The position of the transition on the crossplot separates the producing formations of this report by age, depositional environment, and reservoir characteristics. Crossing the transition from left to right in the direction of increasing clay content marks the onset of a rapid decline in porosity and gas production. In addition, the slope break at 80 API units separates apparent positive and negative influences of clay on reservoir characteristics.

Generally, the effects of clay on porosity and gas production are unfavorable, reducing overall porosity and permeability by occupying pores, filling pore networks by deforming during burial (Schmoker, 1997), and destroying permeability by expanding and mobilizing during production. In some cases, however, clay appears to be somewhat beneficial to both porosity and gas production. Some clay types, if not present in amounts that seriously degrade permeability, might "bind" water that would otherwise be produced and in moderate amounts can actually preserve porosity (and perhaps permeability) by retarding quartz cementation (Schmoker, 1997).

Schmoker (1997, his fig. 5) showed that higher porosity (normalized for the level of thermal maturity) in the Lower Cretaceous J sandstone (Dakota Group) of the Denver Basin, Colorado, is associated with intermediate clay content (≈12 volume percent) and that porosity declines as clay content increases or decreases. The data of this report indicate a similar porosity trend and show that gas production in the northern Great Plains is closely linked to both porosity and clay content.

Figures 9 and 10 show compensated density porosity and volume of production in the peak calendar year, respectively, plotted against clay volume (GR). Among other trends, the two figures show that porosity and gas production covary with clay content. Both variables increase from lower levels to peak at ≈60 API units, a clay volume consistent with that of the highest porosity values of Schmoker (1997), ≈12 percent. Above ≈17 volume percent clay (fig. 8; 80 API units), the suggested transition point between grain- and matrix-supported lithologies, maximum porosity and production decline rapidly. Thus, the optimum clay content for higher porosity in the J sandstone, as suggested by Schmoker (1997), also appears to be the optimum clay content for maximum porosity and gas production in the Cretaceous of the northern Great Plains and ranges from ≈7 to 17 volume percent clay (50–80 API units). Schmoker's data also show that porosity may be more rapidly reduced by increasing clay content than by increasing thermal maturation. Therefore, at a given level of thermal maturity, clay-content measurements may provide an additional level of detail for porosity prediction, above that attained by using thermal maturation alone (Schmoker and Hester, 1990).

Clay-rich, low-permeability sandstones (or siltstones) generally have low effective porosity. In contrast, producing intervals tend to be those that retain higher-than-normal porosity as thermal maturity (Hester, 1997) and (or) clay content increases. The data of figure 9 show that for gas-producing intervals of this report, overall porosity decline with increasing clay content is negligible ($r^2 = 0.03$). The lack of porosities below 8 percent reflects the economic and geologic biases of the producing-interval data and suggests that effective porosities of <8 percent are probably inadequate for commercial gas production regardless of clay content. As the transition from grain-supported to matrix-supported lithology advances beyond a clay volume of ≈35 percent (130 API units), the minimum effective porosity required for gas production increases rapidly. As a result, the number of potential producing intervals declines significantly (fig. 9). The data of figures 9 and 10, in conjunction with the data of Schmoker (1997), suggest that commercial gas production from intervals where clay volume exceeds 50 percent (175 API units) is rare.

Lower-clay-content intervals within a particular zone of interest commonly have better porosity and permeability than do adjacent higher-clay-content rocks. The cleanest intervals, therefore, best characterize the production potential for any given zone or formation, in a given well. In this way, intervals from various geologic environments may be compared, and their potential for gas production assessed, by using the N – D versus GR crossplot and the resulting GPI (figs. 3 and 8). It bears repeating that the GPI empirically combines porosity, water saturation, and clay content into a single parameter that associates the in situ rock with the potential to produce gas. Use of the GPI may be favorably compared with direct well-testing methods such as absolute open-flow potential (AOF). AOF was used to evaluate individual well productivity for the Eagle Sandstone of the Cedar Creek anticline, southeast Montana (Green, 1997). AOF was calculated after all perforated intervals were stimulated and a final flow test was conducted. A strong correlation ($r^2 = 0.88$) of AOF with best 12-month cumulative gas production (Green, 1997, his fig. 5)

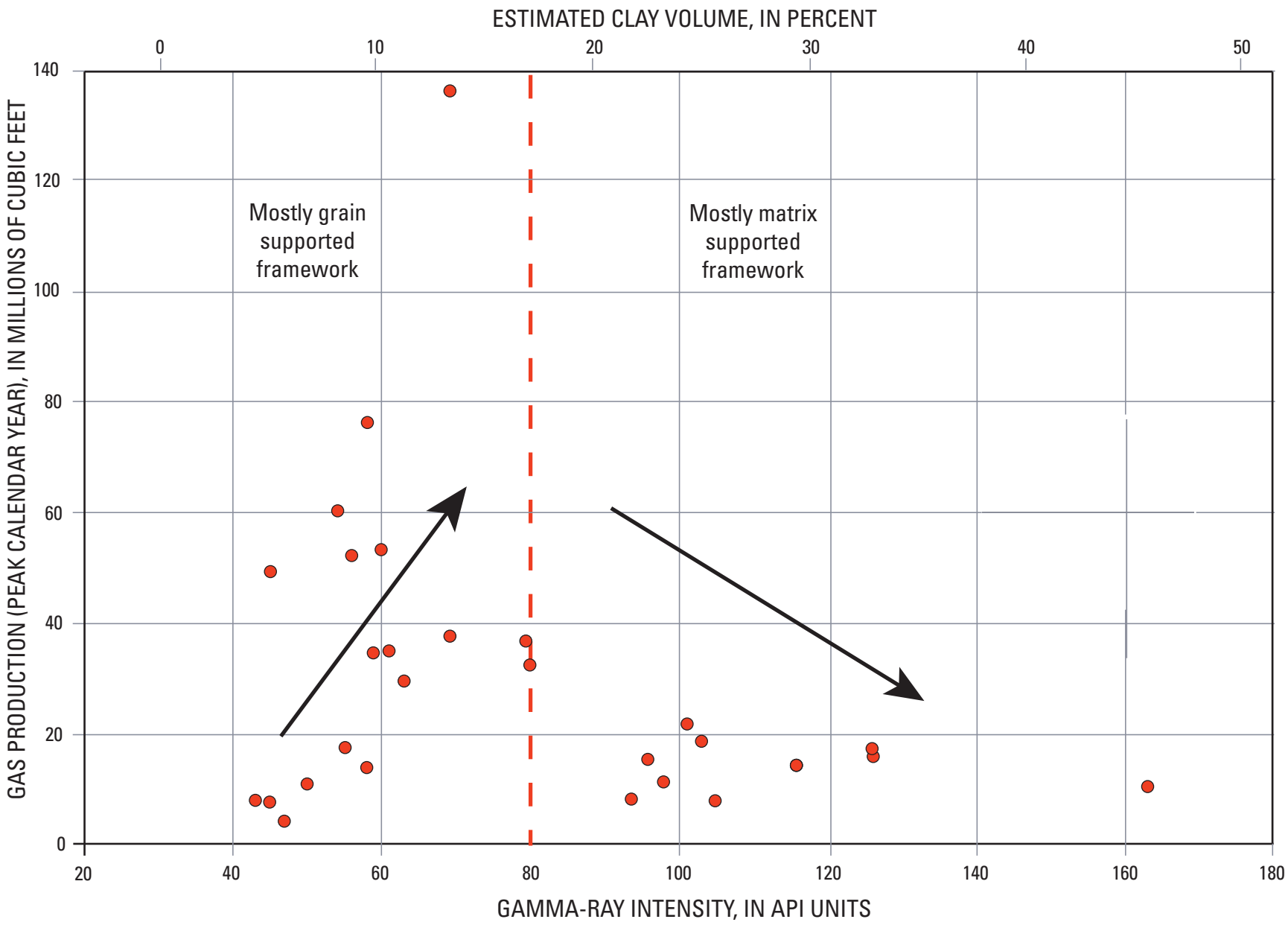

Figure 10. Gas production (peak calendar year) versus gamma-ray intensity for 28 wells (159 intervals; marked with asterisks in Table 1) in northern Montana. Gamma-ray intensity for each well is averaged from its constituent intervals. The number of intervals perforated (per well) is given in table 1. Approximate transition (80 API units) between mostly grain supported and mostly matrix supported framework is dashed. Wells are located in figure 1 and identified in table 1. Estimated clay volume is scaled opposite gamma-ray intensity (*x*-axis).

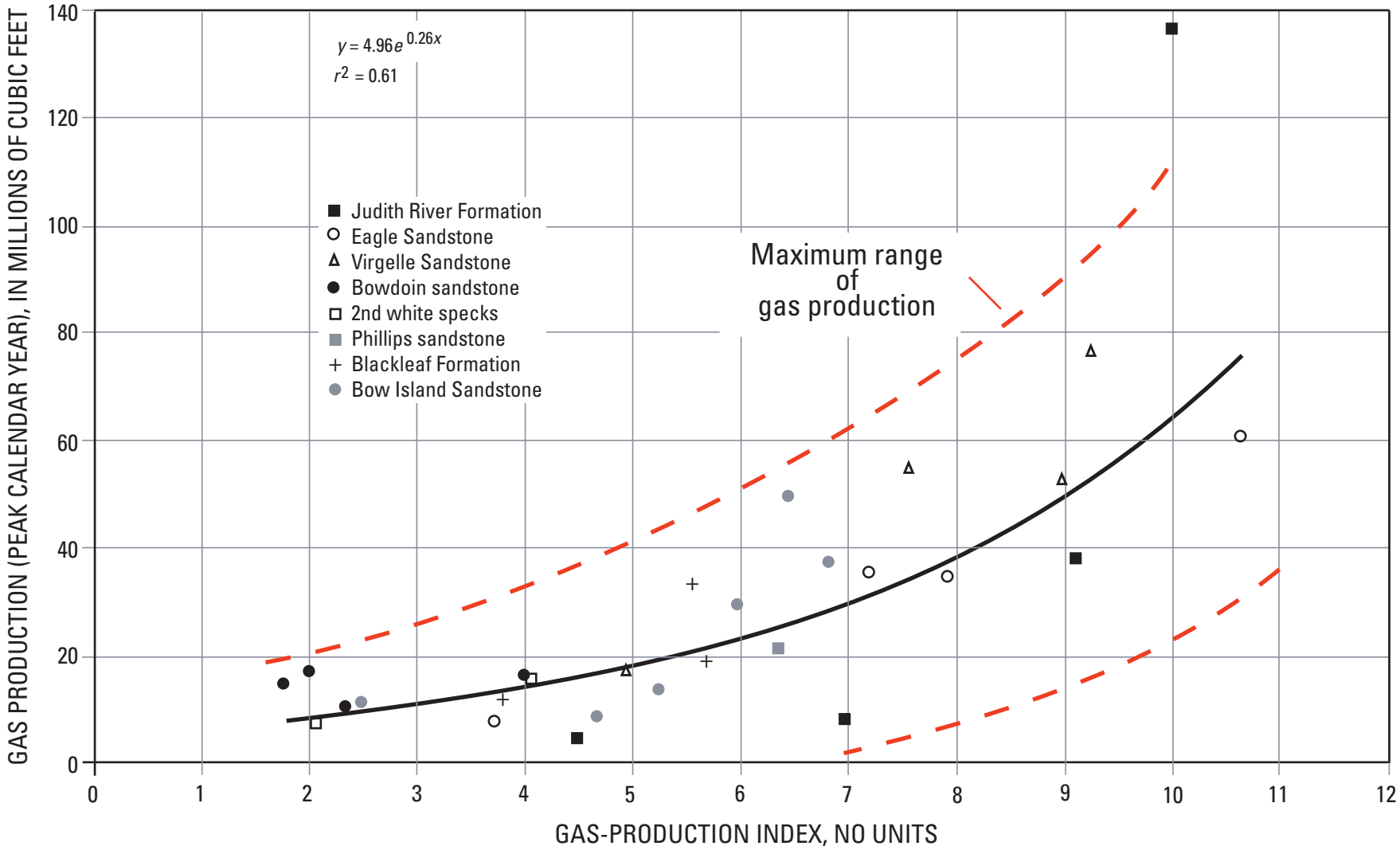

Figure 11. Gas production (peak calendar year) versus gas-production index (GPI) for 28 wells (159 intervals; marked with asterisks in Table 1) in northern Montana. GPI for each well is averaged from its constituent intervals, by using the calibration system of figures 3 and 8. The number of intervals perforated (per well) is given in table 1. Upper dashed line indicates approximate maximum range of production associated with a given GPI level. Wells are located in figure 1 and identified in table 1. Equation and sample coefficient of determination (r^2) for regression line are shown in upper left corner.

suggests that AOF testing in this way can be a good indicator of longer-term well performance in the Eagle Sandstone. By comparison, the GPI, which is a similar measure of cumulative gas production (fig. 11, $r^2 = 0.61$), also appears to be a good indicator of longer-term well performance.

Figure 11 shows volume of production in the peak calendar year plotted against the GPI for each of 28 gas-producing wells of this report (fig. 1; table 1). The GPI for each well is an average of its constituent intervals. The sample coefficient of determination ($r^2 = 0.61$) shows a strong dependence of gas production on the GPI. Geologic variables not directly measured by porosity and gamma-ray logs, such as natural fractures and the differentiation of clay-mineral species, are not accounted for but are manifested as scatter about the regression line of figure 11. The potential for production is shown by the range (dashed lines) associated with a given GPI value. To the extent that the data are representative of the geology and productivity of the northern Great Plains in general, figure 11 reflects typical production rates reasonably expected for a given quality of reservoir rock or producing interval, as measured by the GPI.

Algorithms for Generating GPI Values

The algorithms (appendixes 1 and 2) are made up of multiple parts. Each part consists of a brief description and an equation or equivalence. The syntax and mode of operation for the algorithms are different for different computer applications and, therefore, are discussed separately. Two applications are discussed—Geographix's Prizm, a log-analysis program

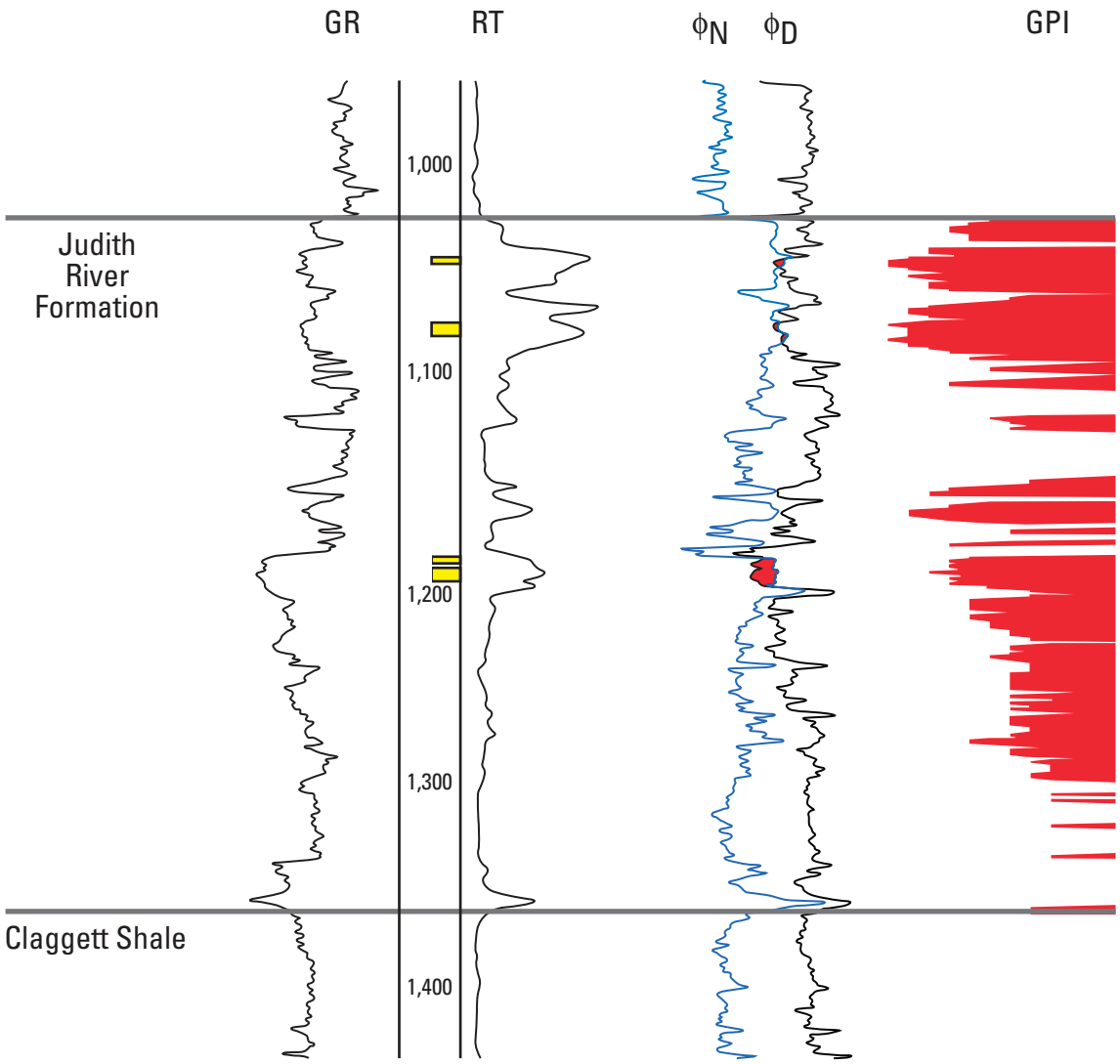

Figure 12. Prizm results for well no. 2 (table 1; fig. 1), showing typical log responses and calculated GPI curve (red) for Cretaceous Judith River Formation, north-central Montana. This well produced 37.9 million cubic feet of gas in its best year of production. Perforated intervals (yellow) are shown in depth track (depths are in feet). Red fill between neutron- and density-porosity curves illustrates typical gas-effect crossover.

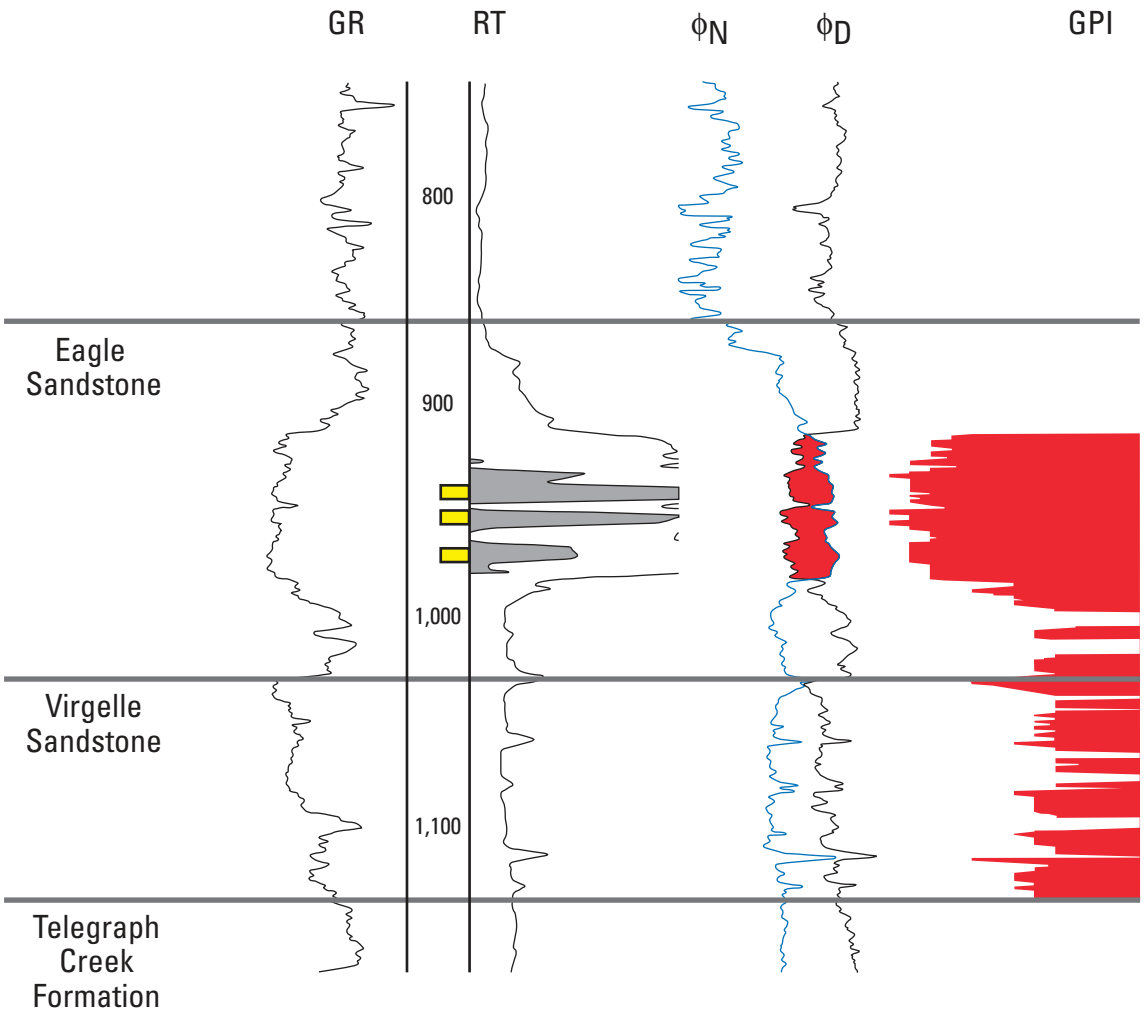

Figure 13. Prizm results for well no. 6 (table 1; fig. 1), showing typical log responses and calculated GPI curve (red) for Cretaceous Eagle Sandstone, north-central Montana. This well produced 60.3 million cubic feet of gas in its best year of production. Perforated intervals (yellow) are shown in depth track (depths are in feet). Red fill between neutron- and density-porosity curves illustrates typical gas-effect crossover. RT backup curves (dark gray–shaded peaks) are shown to left of main RT curve.

specifically designed for digital well-log files, and Microsoft's Excel spreadsheet software. The algorithms either retrieve data directly from digital logs (Prizm) or from log data entered into rows and columns (Excel). The significant differences between the two applications are that Prizm is relatively simple to program and can generate the GPI values and the log traces shown in figures 12, 13, and 14. Excel is more complicated to program and can only generate the GPI values. Prizm, therefore, is the more powerful and robust and is the application of choice.

The algorithm calculates the GPI by using a series of Boolean (If ... Then ... Else) statements to define an area on the crossplot to represent a specific numerical index level (figs. 3 and 8). The boundaries for each index level are the line segments shown in figures 3, 8, and 15 and are represented in the algorithm by their unique equations (given in fig. 15). For each data point plotted on the crossplot, a GPI value is assigned on the basis of the plotted point's position on the crossplot. The following paragraphs describe how the digital data, the equations for the lines, and Boolean logic are used by the two algorithms to generate the GPI.

Using the Algorithm in Prizm

Three log curves are used by Prizm to calculate the GPI: density porosity, neutron porosity, and gamma-ray intensity. Density-porosity values may be taken directly from the density-porosity curve or calculated from bulk density by using the equation

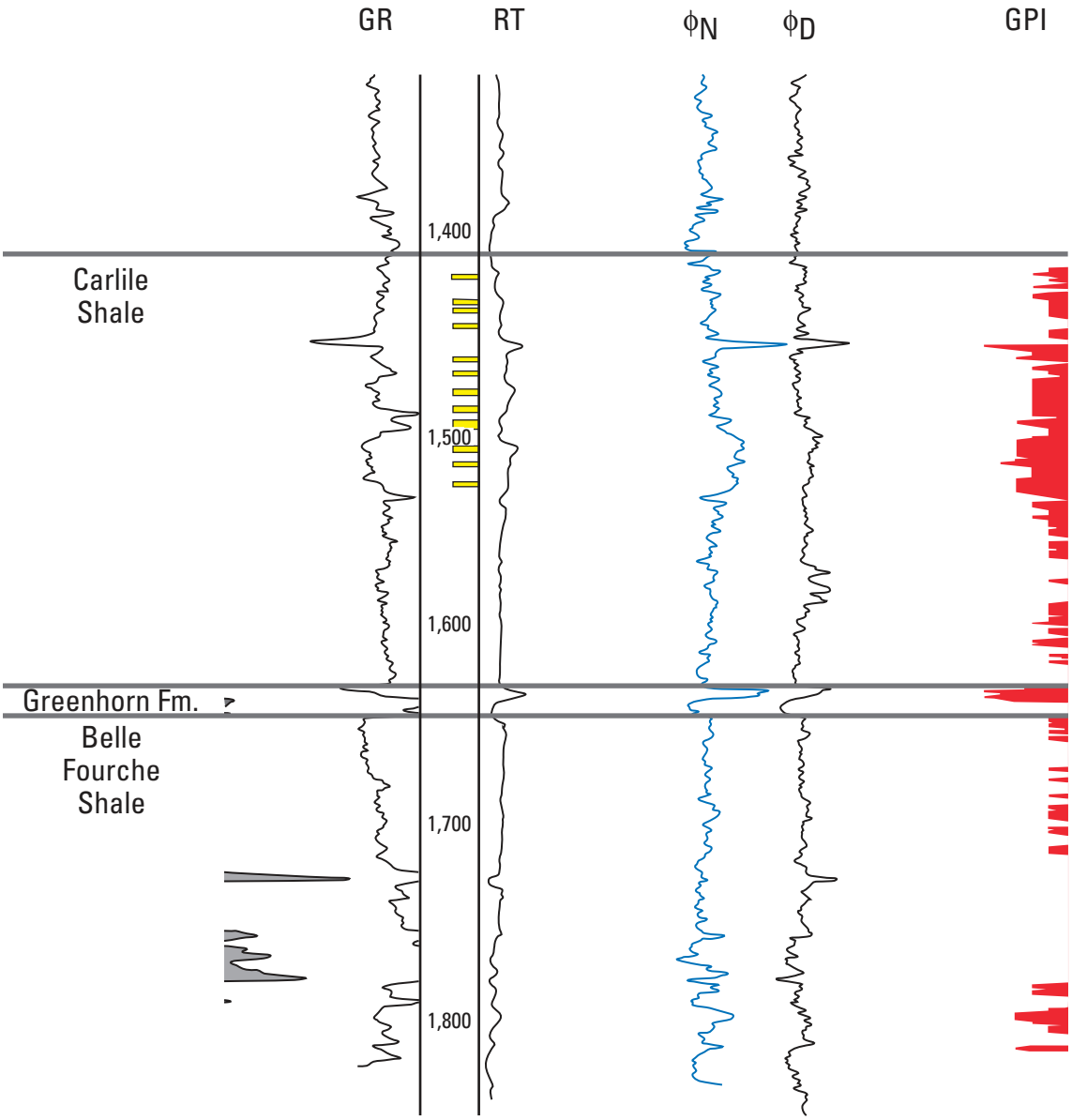

Figure 14. Prizm results for well no. 34 (table 1; fig. 1), showing typical log responses and calculated GPI curve (red) for Cretaceous Carlile Shale (Bowdoin sandstone), Greenhorn Formation (2nd white specks), and Belle Fourche Shale (Phillips sandstone), north-central Montana. This well produced 14.6 million cubic feet of gas in its best year of production. Perforated intervals (yellow) are shown in depth track (depths are in feet). GPI curve illustrates sensitivity of the N – D versus GR crossplot to gas in a clay-rich environment when no gas-effect crossover occurs on the logs. Gamma-ray backup (dark gray–shaded peaks) is shown to left of gamma-ray curve.

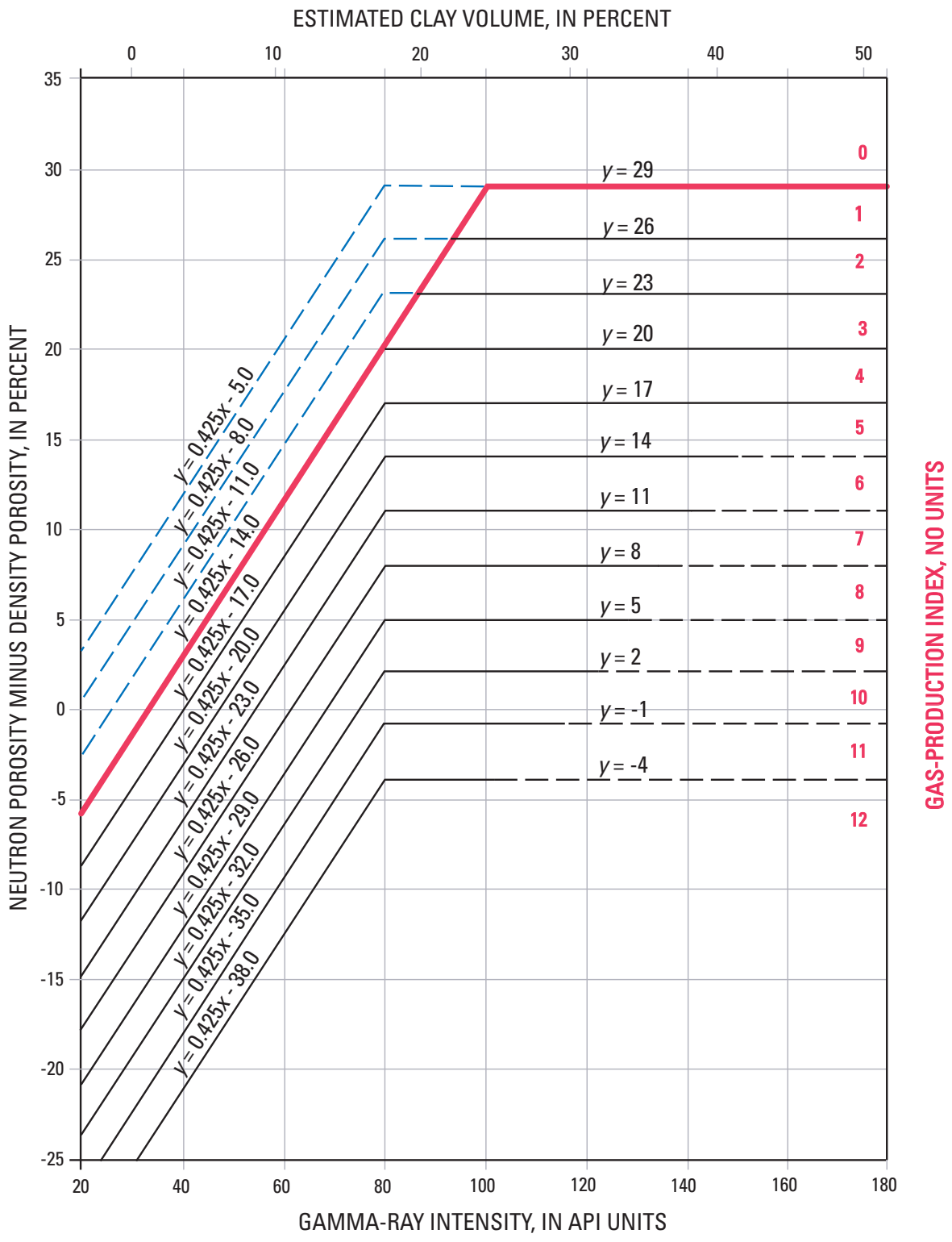

Figure 15. Neutron porosity minus density porosity versus gamma-ray intensity crossplot, showing equations for line segments that make up the gas-production index (GPI). Intervals between thin, solid lines show 12 indexed levels of gas-production potential. Level 1 indicates the least potential for gas production; level 12 indicates the greatest potential. Bold red line is an empirically determined economic limit, with a GPI of zero, above which commercial volumes of gas are unlikely. Dashed lines are inferred.

$$\phi_{density} = (\rho_{ma} - \rho_b)/(\rho_{ma} - \rho_f) , \quad (7)$$

where

$\phi_{density}$ = density porosity (percent/100),
ρ_{ma} = matrix density (grams per cubic centimeter; g/cm^3),
ρ_b = bulk density (g/cm^3), and
ρ_f = fluid density (g/cm^3).

Whatever the source, density porosity should be converted to porosity units for consistency with the porosity display in this application (fig. 15, *y*-axis) by using the equation

$$\phi_D = \phi_{density} \times 100 , \quad (8)$$

where

ϕ_D = density porosity in porosity units.

Similarly, neutron porosity recorded as decimal percent should also be converted to porosity units:

$$\phi_N = \phi_{neutron} \times 100 . \quad (9)$$

Density porosity is then subtracted from neutron porosity to yield a single variable (ϕ_{ND}) for "neutron porosity minus density porosity":

$$\phi_{ND} = \phi_N - \phi_D . \quad (10)$$

The linear equations for the line segments are of the form

$$y = mx + b , \quad (11)$$

where

y = the variable "neutron porosity minus density porosity" (ϕ_{ND}, *y*-axis, fig. 15),
x = the variable "gamma-ray intensity" (GR, *x*-axis, fig. 15),
m = the slope of the line segment, and
b = the *y*-intercept at $x = 0$.

For this application, all lines are parallel; thus each has the same slope (0.425 or zero, depending on the segment); the *y*-intercept is different for each line. The values for the variable ϕ_{ND} are generated from the digitized neutron- and density-porosity curves (equations 7–9); GR is taken directly from the digitized gamma-ray curve.

Lines on the Left Side of the Crossplot

Now the algorithm can be written for the equations for the lines on the left side of the crossplot (where GRI < 80 API units) on the basis of If ... Then ... Else statements and the equations for the lines on the left side of figure 15. The If ... Then ... Else statements are written here by using the general form

$$\text{If } (y > (m \times x) + b) \text{ Then } X_n = X_{n-1} \text{ Else } X_n = n , \quad (12)$$

where

X = a variable representing the value of GPI (with a range of $n = 1$ to $n = 12$) for the lines on the left side of the crossplot.

[Note: in equation 13, where $n = 1$, X_{n-1} (that is, X_0) is set equal to zero.] The actual syntax used for the algorithm in Prizm is shown in appendix 1. The equations for the 12 index levels (left side of crossplot) then become the following:

$$\text{If } (\phi_{ND} > (0.425 \times GRI) - 5.0) \quad \text{Then } X_1 = 0 \quad \text{Else } X_1 = 1 \quad (13)$$

$$\text{If } (\phi_{ND} > (0.425 \times GRI) - 8.0) \quad \text{Then } X_2 = X_1 \quad \text{Else } X_2 = 2 \quad (14)$$

$$\text{If } (\phi_{ND} > (0.425 \times GRI) - 11.0) \quad \text{Then } X_3 = X_2 \quad \text{Else } X_3 = 3 \quad (15)$$

$$\text{If } (\phi_{ND} > (0.425 \times GRI) - 14.0) \quad \text{Then } X_4 = X_3 \quad \text{Else } X_4 = 4 \quad (16)$$

$$\text{If } (\phi_{ND} > (0.425 \times GRI) - 17.0) \quad \text{Then } X_5 = X_4 \quad \text{Else } X_5 = 5 \quad (17)$$

$$\text{If } (\phi_{ND} > (0.425 \times GRI) - 20.0) \quad \text{Then } X_6 = X_5 \quad \text{Else } X_6 = 6 \quad (18)$$

$$\text{If } (\phi_{ND} > (0.425 \times GRI) - 23.0) \quad \text{Then } X_7 = X_6 \quad \text{Else } X_7 = 7 \quad (19)$$

$$\text{If } (\phi_{ND} > (0.425 \times GRI) - 26.0) \quad \text{Then } X_8 = X_7 \quad \text{Else } X_8 = 8 \quad (20)$$

$$\text{If } (\phi_{ND} > (0.425 \times GRI) - 29.0) \quad \text{Then } X_9 = X_8 \quad \text{Else } X_9 = 9 \quad (21)$$

$$\text{If } (\phi_{ND} > (0.425 \times GRI) - 32.0) \quad \text{Then } X_{10} = X_9 \quad \text{Else } X_{10} = 10 \quad (22)$$

$$\text{If } (\phi_{ND} > (0.425 \times GRI) - 35.0) \quad \text{Then } X_{11} = X_{10} \quad \text{Else } X_{11} = 11 \quad (23)$$

$$\text{If } (\phi_{ND} > (0.425 \times GRI) - 38.0) \quad \text{Then } X_{12} = X_{11} \quad \text{Else } X_{12} = 12 . \quad (24)$$

Lines on the Right Side of the Crossplot

Now the algorithm can be written for the equations for the lines on the right side of the crossplot (where GR > 80 API units), again on the basis of If ... Then ... Else statements and the equations for the lines on the right side of figure 15. The general form is the same as equation 11 except that the lines on the right side have zero slope ($m = 0$), and therefore $y = b$. The general form (equation 12) is now simplified to the following statement:

$$\text{If } (y > b) \text{ Then } Y_n = Y_{n-1} \text{ Else } Y_n = n\ , \qquad (25)$$

where

Y = a variable representing the value of GPI (with a range of $n = 1$ to $n = 12$) for the right side of the crossplot.

[Note: in the first line where $n = 1$, Y_{n-1} (that is, Y_0) is set equal to zero.] The actual syntax used for the algorithm in Prizm is shown in appendix 1. The equations for the 12 index levels (right side of crossplot) then become the following:

$$\text{If } (\phi_{ND} > 29) \quad \text{Then } Y_1 = 0 \quad \text{Else } Y_1 = 1 \qquad (26)$$

$$\text{If } (\phi_{ND} > 26) \quad \text{Then } Y_2 = Y_1 \quad \text{Else } Y_2 = 2 \qquad (27)$$

$$\text{If } (\phi_{ND} > 23) \quad \text{Then } Y_3 = Y_2 \quad \text{Else } Y_3 = 3 \qquad (28)$$

$$\text{If } (\phi_{ND} > 20) \quad \text{Then } Y_4 = Y_3 \quad \text{Else } Y_4 = 4 \qquad (29)$$

$$\text{If } (\phi_{ND} > 17) \quad \text{Then } Y_5 = Y_4 \quad \text{Else } Y_5 = 5 \qquad (30)$$

$$\text{If } (\phi_{ND} > 14) \quad \text{Then } Y_6 = Y_5 \quad \text{Else } Y_6 = 6 \qquad (31)$$

$$\text{If } (\phi_{ND} > 11) \quad \text{Then } Y_7 = Y_6 \quad \text{Else } Y_7 = 7 \qquad (32)$$

$$\text{If } (\phi_{ND} > 8) \quad \text{Then } Y_8 = Y_7 \quad \text{Else } Y_8 = 8 \qquad (33)$$

$$\text{If } (\phi_{ND} > 5) \quad \text{Then } Y_9 = Y_8 \quad \text{Else } Y_9 = 9 \qquad (34)$$

$$\text{If } (\phi_{ND} > 2) \quad \text{Then } Y_{10} = Y_9 \quad \text{Else } Y_{10} = 10 \qquad (35)$$

$$\text{If } (\phi_{ND} > -1) \quad \text{Then } Y_{11} = Y_{10} \quad \text{Else } Y_{11} = 11 \qquad (36)$$

$$\text{If } (\phi_{ND} > -4) \quad \text{Then } Y_{12} = Y_{11} \quad \text{Else } Y_{12} = 12\ . \qquad (37)$$

Now the left and right sides of the crossplot are combined by using the following statement:

$$\text{If } (\text{GRI} < 80) \quad \text{Then } Z = X_{12} \quad \text{Else } Z = Y_{12}\ . \qquad (38)$$

A “discriminator” statement is now added to create a “GPI = zero” line that passes through both sides of the crossplot (fig. 15; heavy, red diagonal line). This line is established empirically (by using gas-production data) and defines a boundary, above which commercial volumes of gas are not likely to be produced (Hester, 1999a).

$$\text{If } (\phi_{ND} > (0.425 \times \text{GRI}) - 14.0) \quad \text{Then GPI} = 0 \quad \text{Else GPI} = Z\ . \qquad (39)$$

	A	B	C	D	E	F	G	H	I	J	K
1	Well #	Int #	Gr	N-D	Left Top	Left Bot	Right Top	Right Bot	Left GPI	Right GPI	Final GPI
2	1	1	45	-6.2	7	-999.25	FALSE	12	7	12	7
3	2	1	42	-0.2	5	-999.25	FALSE	10	5	10	5
4	2	2	52	5.7	4	-999.25	FALSE	8	4	8	4
5	4	1	81	-2.6	FALSE	11	FALSE	11	11	11	11
6	4	2	79	-1.1	10	-999.25	FALSE	11	10	11	10
7	4	3	49	-5.5	8	-999.25	FALSE	12	8	12	8
8	6	1	61	-4.5	9	-999.25	FALSE	12	9	12	9
9	6	2	70	-4.9	10	-999.25	FALSE	12	10	12	10
10	6	3	68	-3.6	10	-999.25	FALSE	11	10	11	10
11	6	4	70	-2.8	10	-999.25	FALSE	11	10	11	10
12	6	5	75	-3.6	FALSE	11	FALSE	11	11	11	11
13	8	1	63	-4.8	9	-999.25	FALSE	12	9	12	9
14	8	2	64	3.8	7	-999.25	FALSE	9	7	9	7
15	8	3	66	-3.6	9	-999.25	FALSE	11	9	11	9
16	8	4	57	1.7	6	-999.25	FALSE	10	6	10	6
17	8	5	56	-1.6	7	-999.25	FALSE	11	7	11	7
18	8	6	55	3.1	6	-999.25	FALSE	9	6	9	6
19	8	7	56	-2.5	8	-999.25	FALSE	11	8	11	8
20	9	1	63	-7	10	-999.25	FALSE	12	10	12	10
21	9	2	52	-20.2	FALSE	12	FALSE	12	12	12	12
22	9	3	60	0.7	7	-999.25	FALSE	10	7	10	7
23	10	1	56	-5.7	9	-999.25	FALSE	12	9	12	9
24	11	1	55	4.1	5	-999.25	FALSE	9	5	9	5
25	11	2	54	3.2	5	-999.25	FALSE	9	5	9	5
26	12	1	124	28.5	7	-999.25	1	-999.25	7	1	1
27	12	2	120	27.5	7	-999.25	1	-999.25	7	1	1
28	12	3	117	27.7	6	-999.25	1	-999.25	6	1	1
29	12	4	122	25.1	8	-999.25	2	-999.25	8	2	2
30	12	5	116	24.3	7	-999.25	2	-999.25	7	2	2
31	12	6	135	25.1	10	-999.25	2	-999.25	10	2	2
32	12	7	108	22.2	7	-999.25	3	-999.25	7	3	3
33	12	8	113	23.4	7	-999.25	2	-999.25	7	2	2
34	12	9	100	17.9	7	-999.25	4	-999.25	7	4	4
35	12	10	107	28.7	4	-999.25	1	-999.25	4	1	1

Figure 16. Example of Excel spreadsheet with 34 records of well data (columns A and B) and interval data (columns C and D). Completed calculations (or "answers") are shown in the cells of columns E through K. Procedure for inserting formulas and data is shown in appendix 2.

Other parameters may be added to this statement to further discriminate by using minimum or maximum values. Examples might include some of the following: (1) eliminating from the calculations all porosities below 8 percent by using the density-porosity curve, (2) creating "zoned" parameters that can change matrix densities for certain stratigraphic intervals, or (3) eliminating shaly zones from the calculations by using the gamma-ray curve. Appendix 1 shows examples of additional discriminators that were used in evaluating gas wells in north-central Montana (Hester, 1999c, 1999d). The code in appendix 1 will generate the GPI when copied to a user's computer clipboard and pasted into Prizm's "User-Defined Equations" window.

Using the Algorithm in Excel

The algorithm is used in Excel by applying a series of "nested" If ... Then ... Else statements. The statements and the values for neutron and density porosities and gamma-ray intensity are written into cells in specific columns. Each row constitutes a single data point (record). Raw data can be entered by hand or copied from the digitized-log files once the header data and unnecessary curve data are removed (it is wise to save a copy of the original digitized-log file).

One caveat of using this method is that Excel (Office 97) allows for a maximum of only eight If ... Then ... Else statements in a single cell. Because there are 12 levels of GPI (each requiring an If ... Then ... Else statement), the equations for both left and right sides of the crossplot (12 statements each; fig. 15) must be separated into multiple columns to do the calculations and then recombined.

The procedure requires that the statements representing the equations for the lines on the left side of the crossplot be split into two groups, "top" and "bottom." The calculations for each group are completed, and then the groups are recombined to put the GPI values for the left side of the crossplot into a single column. The equations for the right side of the crossplot are handled in the same way. Finally, the GPI values for the left and right sides of the crossplot are combined (final GPI).

Appendix 2 explains the procedure for inserting the formulas and data into an Excel spreadsheet. Figure 16 is an example of an Excel spreadsheet with 34 records of well data (columns A and B) and interval data (columns C and D). Completed calculations (or "answers") are shown in the cells of columns E through K.

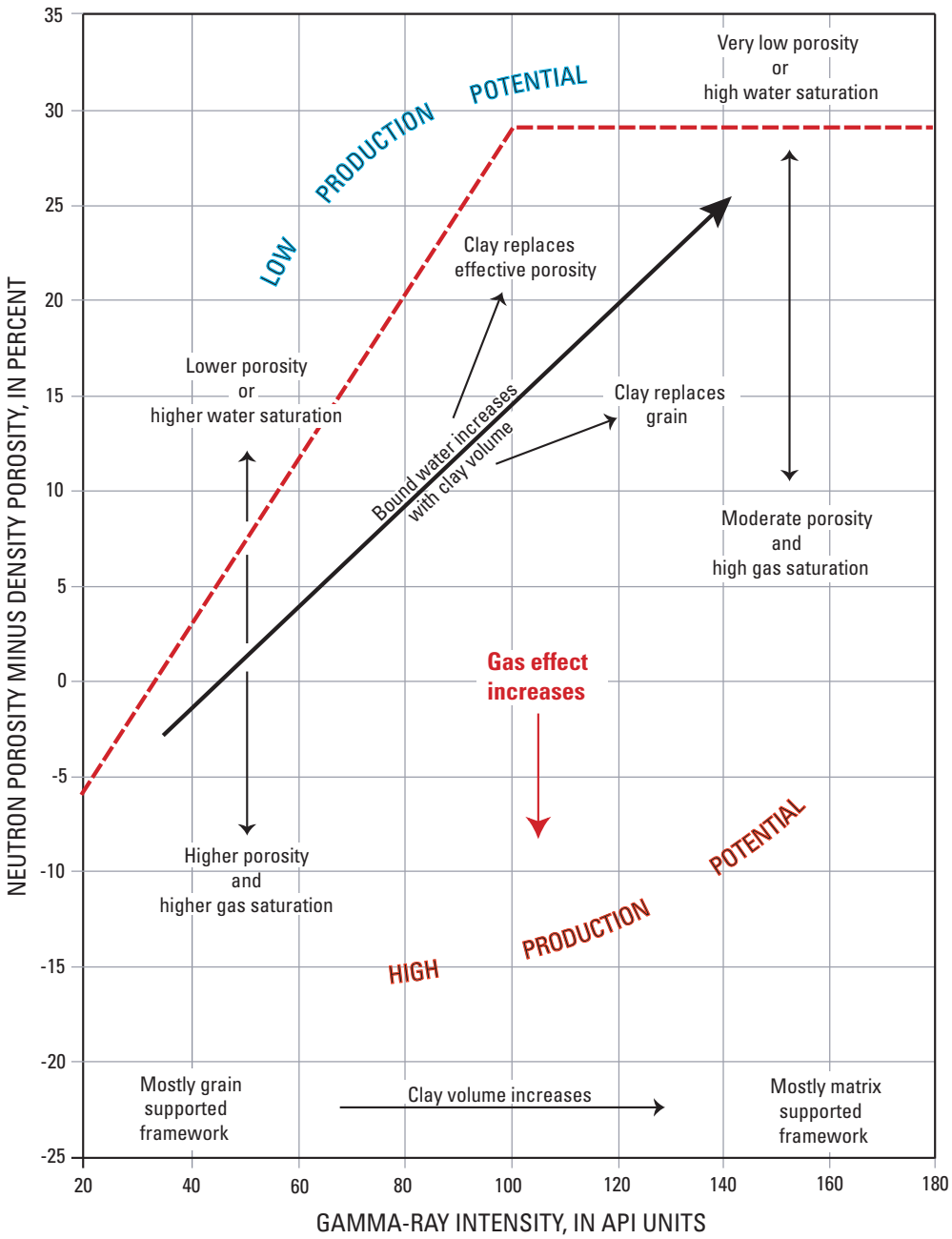

Figure 17. Summary crossplot of neutron porosity minus density porosity versus gamma-ray intensity, showing relative variation in porosity, water saturation, clay volume, bound water, and production potential with plotted position of interval data. Heavy solid line is linear-regression line for interval data of figure 7, showing relationship of bound water to increasing clay content. Dashed line is zero-production baseline (that is, GPI = 0) of figures 3, 8, and 15.

Summary

In the northern Great Plains, the potential exists for large volumes of biogenic methane within only a few thousand feet of the surface. Although limited areas have been exploited, vast areas remain undeveloped. One of the primary reasons for the lack of development is the difficulty in recognizing and evaluating gas-charged reservoirs. Unconventional, continuous-type, gas-charged lithologies, such as those in the northern Great Plains, are commonly unrecognizable on geophysical well logs and are therefore not well suited to conventional methods of formation evaluation. Potential producing intervals are thus overlooked.

A calibration system developed here (figs. 3, 8, and 15) simplifies identification, evaluation, and selection of potential gas-producing intervals in the varying geologic settings of the Cretaceous of the northern Great Plains. Geologic parameters targeted by conventional log analyses—such as effective porosity, water saturation, and clay content—are accounted for empirically by using a single gas-production index (GPI), which links the gas effect directly with production. Intervals from different formations (or wells) can be compared with each other, on the same plot, in the context of production potential and geologic variation. Figure 17 summarizes and illustrates the influence of variations in porosity and water saturation, clay volume, bound water, and the gas effect, on the relative positions of plotted interval data.

Intervals that plot below the zero-production baseline (fig. 8) have a higher potential to produce gas than those that plot above that baseline. The potential for production increases as N – D (*y*-axis, figs. 3, 8, and 15) decreases. Geologic and engineering factors, however—such as natural fractures and well-completion techniques—can significantly influence well productivity. Data from Campen (1975) indicate that some water production can occur at GPI levels of ≤7. In addition, the overall success ratio (Schmoker, 1995) for gas wells in many areas of north-central Montana is projected to be as low as 50 percent (Rice and Spencer, 1995). Nevertheless, the calibration system described in this report is a robust indicator of gas-production potential. The gas-production index (GPI) constitutes an interpretative tool that should be considered in conjunction with (or in lieu of) conventional formation evaluation.

Selected References

Campen, E.B., 1975, Well log analysis in the Cretaceous gas sands of northern Montana, *in* Doroshenko, J., Miller, W.R., Thompson, E.E., and Rawlins, J.H., eds., Energy resources of Montana: Billings, Mont., Montana Geological Society 22nd Annual Publication, p. 15–25.

Condon, S.M., Ridgley, J.L., Rowan, E.L., Anna, L.O., Lillis, P.G., Hester, T.C., and Cook, Troy, 2000, Re-evaluation of controls on Cretaceous shallow biogenic gas accumulations, northern Great Plains, U.S.A., and southeast Alberta and southwest Saskatchewan, Canada, *in* Schalla, R.C., and Johnson, E.H., eds., Montana/Alberta thrust belt and adjacent foreland, Volume II, Road logs, presentation abstracts, and foothills analyses: Billings, Mont., Montana Geological Society 50th Anniversary Symposium, p. 5–8.

Cutress, W.G., 1974, An empirical approach to log interpretation in the Viking sand of east central Alberta: Houston, Tex., Society of Professional Well Log Analysts Fifteenth Annual Logging Symposium Transactions, p. G1–G17.

Dyman, T.S., Peterson, J.A., Schmoker, J.W., Spencer, C.W., Rice, D.D., Porter, K.W., Lopez, D.A., Heck, T.J., and Beeman, W.R., 1995, Assessment of undiscovered resources in petroleum plays: U.S. portion of Williston basin and north-central Montana: Billings, Mont., Seventh International Williston Basin Symposium, p. 323–339.

Green, T., 1997, Shallow gas completions benefit from advanced stimulation technology: Rockville, Md., Gas Research Institute, Gas TIPS, Winter 1996/1997, p. 14–19.

Henry, K.C., 1979, Gas detection in the extremely shaly Bowdoin Formation of northern Montana: Houston, Tex., Society of Professional Well Log Analysts Twentieth Annual Logging Symposium Transactions, p. T1–T9.

Heslop, A., 1974, Gamma-ray log response of shaly sandstones: Houston, Tex., Society of Professional Well Log Analysts Fifteenth Annual Logging Symposium Transactions, p. M1–M11.

Hester, T.C., 1997, Porosity trends of Pennsylvanian sandstones with respect to thermal maturity and thermal regimes in the Anadarko Basin, Oklahoma, *in* Dyman, T.S., Rice, D.D., and Westcott, W.A., eds., Geologic controls of natural gas in deep sedimentary basins in the United States: U.S. Geological Survey Bulletin 2146-I, p. 105–124.

Hester, T.C., 1999a, Prediction of gas production using well logs, Cretaceous of north-central Montana: Mountain Geologist, v. 36, no. 2, p. 85–97.

Hester, T.C., 1999b, Calibration of the “gas effect” using neutron, density, and gamma-ray-intensity wire-line logs: U.S. Geological Survey Open-File Report 99-128, 23 p.

Hester, T.C., 1999c, Log-derived, regional evaluation of gas-production potential, Cretaceous of northern Montana: American Association of Petroleum Geologists Annual Convention Program with Abstracts, p. A-59.

Hester, T.C., 1999d, The “gas effect” as an indicator of gas-production potential, Cretaceous of north-central Montana: Tulsa, Okla., American Association of Petroleum Geologists [AAPG], Rocky Mountain Section Meeting, Program with Abstracts, p. A5.

Hester, T.C., 2001, An algorithm for estimating gas-production potential using digital wire-line log data (Cretaceous of northern Montana): U.S. Geological Survey Open-File Report 01-12, 22 p.

Kowalchuk, H., Coates, G., and Wells, L., 1974, The evaluation of very shaly formations in Canada using a systematic approach: Houston, Tex., Society of Professional Well Log Analysts Fifteenth Annual Logging Symposium Transactions, p. H1–H21.

Kukal, G.C., 1981, Formation evaluation and gas detection in shallow, low-permeability, shaly sands of the northern Great Plains province: Journal of Petroleum Technology, v. 33, no. 10, p. 1976–1984.

Molenaar, C.M., and Rice, D.D., 1988, Cretaceous rocks of the Western Interior Basin, *in* Sloss, L.L., ed., Sedimentary cover—North American craton: Boulder, Colo., Geological Society of America, Geology of North America, v. D-2, p. 77–82.

Rice, D.D., 1975, Origin of and conditions for shallow accumulations of natural gas: Laramie, Wyo., Wyoming Geological Association 27th Annual Field Conference Guidebook, p. 267–271.

Rice, D.D., 1981, Subsurface cross section from southeastern Alberta, Canada, to Bowdoin dome area, north-central

Montana, showing correlation of Cretaceous rocks and shallow, gas-productive zones in low-permeability reservoirs: U.S. Geological Survey Oil and Gas Investigations Chart OC-112.

Rice, D.D., and Claypool, G.E., 1981, Generation, accumulation, and resource potential of biogenic gas: American Association of Petroleum Geologists Bulletin, v. 65, no. 1, p. 5–25.

Rice, D.D., and Shurr, W.G., 1980, Shallow, low-permeability reservoirs of the northern Great Plains—An assessment of their natural resources: American Association of Petroleum Geologists Bulletin, v. 64, no. 7, p. 969–987.

Rice, D.D., and Spencer, C.W., 1995, Northern Great Plains shallow biogenic gas, *in* Gautier, D.L., Dolton, G.L., Takahashi, K.I., and Varnes, K.L., eds., 1995 National assessment of United States oil and gas resources—Results, methodology, and supporting data: U.S. Geological Survey Digital Data Series DDS-30 [CD-ROM].

Ridgley, J.L., Condon, S.M., Anna, L.O., Hester, T.C., Rowan, E.L., Cook, Troy, and Lillis, P.G., 1999, Re-examination of Cretaceous shallow biogenic gas resources, northern Great Plains, Montana—A multidisciplinary approach: Tulsa, Okla., American Association of Petroleum Geologists [AAPG], Rocky Mountain Section Meeting, Program with Abstracts, p. A9.

Ridgley, J.L., Condon, S.M., Hester, T.C., and Quinn, J.C., 1997, Understanding the shallow biogenic gas play of the northern Great Plains—Using the shallow Canadian biogenic gas play as an analog [abs.]: Laramie, Wyo., Wyoming Geological Association Proceedings Volume, p. 8–9.

Ridgley, J.L., Hester, T.C., Condon, S.M., Anna, L.O., Rowan, E.L., Cook, Troy, and Lillis, P.G., 1999, Re-evaluation of the shallow biogenic gas accumulation, northern Great Plains, U.S.A.—Is the similar gas accumulation in southeastern Alberta and southwestern Saskatchewan a good analog?, *in* Christopher, J.E., Delaney, G.D., Gilboy, C.F., Haidl, F.M., Harper, D.T., and Paterson, D.F., eds., Summary of investigations 1999, Volume 1: Saskatoon, Sask., Saskatchewan Geological Survey, Saskatchewan Energy and Mines, Miscellaneous Report 99-4.1, p. 64–78.

Schlumberger, 1987, Log interpretation principles/applications (2d ed.): Houston, Tex., Schlumberger Educational Services, 198 p.

Schmoker, J.W., 1995, Method for assessing continuous-type (unconventional) hydrocarbon accumulations, *in* Gautier, D.L., Dolton, G.L., Takahashi, K.I., and Varnes, K.L., eds., 1995 National assessment of United States oil and gas resources—Results, methodology, and supporting data: U.S. Geological Survey Digital Data Series DDS-30 [CD-ROM].

Schmoker, J.W., 1997, Porosity predictions in deeply buried sandstones, with examples from Cretaceous formations of the Rocky Mountain region, *in* Dyman, T.S., Rice, D.D., and Westcott, W.A., eds., Geologic controls of natural gas in deep sedimentary basins in the United States: U.S. Geological Survey Bulletin 2146-H, p. 77–104.

Schmoker, J.W., and Hester, T.C., 1990, Regional trends of sandstone porosity vs vitrinite reflectance—A preliminary framework, *in* Nuccio, V.F., and Barker, C.E., eds., Applications of thermal maturity studies to energy exploration: Tulsa, Okla., Society of Economic Paleontologists and Mineralogists, Rocky Mountain Section, p. 53–60.

Segesman, F., and Liu, O., 1971, The excavation effect: Dallas, Tex., Society of Professional Well Log Analysts Twelfth Annual Logging Symposium Transactions, p. H1–H21.

Shurr, G.W., and Ridgley, J.L., 2002, Unconventional shallow biogenic gas systems: American Association of Petroleum Geologists Bulletin, v. 86, no. 11, p. 1939–1969.

Whitney, G., and Ahlbrandt, T.S., 1996, Effects of clays on resistivities of clastic rocks and reservoir performance, *in* Dolly, E.D., and Mullarkey, J.C., eds., Hydrocarbon production from low contrast, low resistivity reservoirs, Rocky Mountain and Mid-Continent regions, log examples of subtle pays: Denver, Colo., Rocky Mountain Association of Geologists Guidebook, p. 43–52.

Appendix 1. Plug-in Algorithm for Calculating GPI Using Prizm

```
;                    Density Porosity from Bulk Density (decimal)
PHID[] = (RhoM - RHOB[]) / (RhoM - RhoF)

;                    Convert Decimal Porosity to Porosity Units (density and neutron porosity)
D[]=PHID[] * 100
N[]=NPHI[] * 100

;                    Neutron Porosity minus Density Porosity (Porosity Units)
ND[] = N[] - D[]

;                    N – D versus GR Crossplot (left side)
If (ND[] > (0.425 * GR[]) - 5.0) Then X1[]=0 Else X1[]=1
If (ND[] > (0.425 * GR[]) - 8.0) Then X2[]=X1[] Else X2[]=2
If (ND[] > (0.425 * GR[]) - 11.0) Then X3[]=X2[]  Else X3[]=3
If (ND[] > (0.425 * GR[]) - 14.0) Then X4[]=X3[]  Else X4[]=4
If (ND[] > (0.425 * GR[]) - 17.0) Then X5[]=X4[]  Else X5[]=5
If (ND[] > (0.425 * GR[]) - 20.0) Then X6[]=X5[]  Else X6[]=6
If (ND[] > (0.425 * GR[]) - 23.0) Then X7[]=X6[]  Else X7[]=7
If (ND[] > (0.425 * GR[]) - 26.0) Then X8[]=X7[]  Else X8[]=8
If (ND[] > (0.425 * GR[]) - 29.0) Then X9[]=X8[]  Else X9[]=9
If (ND[] > (0.425 * GR[]) - 32.0) Then X10[]=X9[]  Else X10[]=10
If (ND[] > (0.425 * GR[]) - 35.0) Then X11[]=X10[] Else X11[]=11
If (ND[] > (0.425 * GR[]) - 38.0) Then X12[]=X11[] Else X12[]=12

;                    N – D versus GR Crossplot (right side)
If (ND[] > 29.0) Then Y1[]=0  Else Y1[]=1
If (ND[] > 26.0) Then Y2[]=Y1[]  Else Y2[]=2
If (ND[] > 23.0) Then Y3[]=Y2[]  Else Y3[]=3
If (ND[] > 20.0) Then Y4[]=Y3[]  Else Y4[]=4
If (ND[] > 17.0) Then Y5[]=Y4[]  Else Y5[]=5
If (ND[] > 14.0) Then Y6[]=Y5[]  Else Y6[]=6
If (ND[] > 11.0) Then Y7[]=Y6[]  Else Y7[]=7
If (ND[] > 8.0) Then Y8[]=Y7[]  Else Y8[]=8
If (ND[] > 5.0) Then Y9[]=Y8[]  Else Y9[]=9
If (ND[] > 2.0) Then Y10[]=Y9[]  Else Y10[]=10
If (ND[] > -1) Then Y11[]=Y10[]  Else Y11[]=11
If (ND[] > -4) Then Y12[]=Y11[]  Else Y12[]=12

;                    N – D versus GR Crossplot (combination)
If (GR[] < 80) Then Z[]=X12[]  Else Z[]=Y12[]

;                    Neutron plus Density (Discriminator curve)
NDplus[]=NPHI[] + PHID[]

;                    Discriminator Curve for Gas Detection Crossplot  (Resistivity curve (RT[]) eliminates values less
;than 5 ohm-meters. Sum of neutron- and density-porosity curves (NDplus[]) eliminates decimal-porosity values
;greater than 0.75. Neutron-porosity curve (NPHI[]) eliminates decimal-porosity values greater than 0.50. Density-
;porosity curve (PHID[]) eliminates decimal-porosity values less than 0.08. GRI (inserted as a "zoned" parameter for
;the gamma-ray curve (GR[]) can be set at any value. Neutron minus density "GPI = 0" curve (ND[]) eliminates all
;values above the "zero-production baseline."
If (RT[] < 5.0 or NDplus[] > 0.75 or NPHI[] > 0.50 or PHID[] < 0.08 or GR[] > GRI or ND[] > (0.425 * GR[]) -
14.0)  Then GPI[]=0 Else GPI[]=Z[]
```

Appendix 2. Four Steps to Calculating Gas-Production Index Using Excel

First: Insert data or formulas into row 2 of spreadsheet (an example of which is shown below) as indicated by the numbers 1 thru 11.

1. Well number (optional)
2. Interval number (optional)
3. Gamma-ray intensity
4. Neutron porosity minus density porosity
5. Insert formula:

=IF(D2>(0.425*C2)-14,”0”,IF(D2>(0.425*C2)-17,”4”,IF(D2>(0.425*C2)-20,”5”,IF(D2>(0.425*C2)-23,”6”,IF(D2>(0.425*C2)-26,”7”,IF(D2>(0.425*C2)-29,”8”,IF(D2>(0.425*C2)-32,”9”,IF(D2>(0.425*C2)-35,”10”))))))))

6. Insert formula:

=IF(D2>(0.425*C2)-35,”-999.25”,IF(D2>(0.425*C2)-38,”11”,”12”))

7. Insert formula:

=IF(D2>(0.425*C2)-14,”0”,IF(D2<(0.425*C2)-14,IF(D2>29,”0”,IF(D2>26,”1”,IF(D2>23,”2”,IF(D2>20,”3”,IF(D2>17,”4”,IF(D2>14,”5”))))))))

8. Insert formula:

=IF(D2>14,”-999.25”,IF(D2>11,”6”,IF(D2>8,”7”,IF(D2>5,”8”,IF(D2>2,”9”,IF(D2>-1,”10”,IF(D2>-4,”11”,”12”)))))))

10. Insert formula: =IF(G2=FALSE,H2,G2)

11. Insert formula: =IF(C2<80,I2,J2)

Second: Enter all data into columns A through D (that is, column numbers 1 through 4).
Third: Copy formula 5 into each cell of column E (that is, column number 5). (To do this, select cell E2, position cursor on bottom right corner (until the cursor becomes a black plus sign), and drag downward to the end of data set.
Fourth: Repeat this procedure for each formula (column numbers 6 through 11).

	A	B	C	D	E	F	G	H	I	J	K
1	Well #	Int #	Gr	N-D	Left Top	Left Bot	Right Top	Right Bot	Left GPI	Right GPI	Final GPI
2	1	2	3	4	5	6	7	8	9	10	11
3											
4											
5											